



HAL
open science

IFN- γ primes bone marrow neutrophils to acquire regulatory functions in severe viral respiratory infections

Florent Creusat, Youenn Jouan, Loïc Gonzalez, Emilie Barsac, Guy Ilango, Roxane Lemoine, Daphnée Soulard, Antoine Hankard, Chloé Boisseau, Antoine Guillon, et al.

► To cite this version:

Florent Creusat, Youenn Jouan, Loïc Gonzalez, Emilie Barsac, Guy Ilango, et al.. IFN- γ primes bone marrow neutrophils to acquire regulatory functions in severe viral respiratory infections. *Science Advances* , 2024, 10 (41), pp.eadn3257. 10.1126/sciadv.adn3257 . hal-04742150

HAL Id: hal-04742150

<https://hal.inrae.fr/hal-04742150v1>

Submitted on 17 Oct 2024

HAL is a multi-disciplinary open access archive for the deposit and dissemination of scientific research documents, whether they are published or not. The documents may come from teaching and research institutions in France or abroad, or from public or private research centers.

L'archive ouverte pluridisciplinaire **HAL**, est destinée au dépôt et à la diffusion de documents scientifiques de niveau recherche, publiés ou non, émanant des établissements d'enseignement et de recherche français ou étrangers, des laboratoires publics ou privés.



Distributed under a Creative Commons Attribution - NonCommercial 4.0 International License



IMMUNOLOGY

IFN- γ primes bone marrow neutrophils to acquire regulatory functions in severe viral respiratory infections

Florent Creusat^{1,2†}, Youenn Jouan^{1,2,3,4†}, Loïc Gonzalez^{1,2†}, Emilie Barsac^{1,2}, Guy Ilango^{1,2}, Roxane Lemoine^{2,5}, Daphnée Soulard⁶, Antoine Hankard^{1,2}, Chloé Boisseau^{1,2}, Antoine Guillon^{1,2,3}, Qiaochu Lin⁷, Carolina de Amat Herbozo⁷, Valentin Sencio⁶, Nathalie Winter⁸, Damien Sizaret^{1,2,9}, François Trottein⁶, Mustapha Si-Tahar^{1,2}, Benoit Briard^{1,2}, Thierry Mallevaey⁷, Christelle Faveeuw^{6‡}, Thomas Baranek^{1,2‡}, Christophe Paget^{1,2*}

Copyright © 2024 the Authors, some rights reserved; exclusive licensee American Association for the Advancement of Science. No claim to original U.S. Government Works. Distributed under a Creative Commons Attribution NonCommercial License 4.0 (CC BY-NC).

Neutrophil subsets endowed with regulatory/suppressive properties are widely regarded as deleterious immune cells that can jeopardize antitumoral response and/or antimicrobial resistance. Here, we describe a sizeable fraction of neutrophils characterized by the expression of programmed death-ligand 1 (PD-L1) in biological fluids of humans and mice with severe viral respiratory infections (VRI). Biological and transcriptomic approaches indicated that VRI-driven PD-L1⁺ neutrophils are endowed with potent regulatory functions and reduced classical antimicrobial properties, as compared to their PD-L1⁻ counterpart. VRI-induced regulatory PD-L1⁺ neutrophils were generated remotely in the bone marrow in an IFN- γ -dependent manner and were quickly mobilized into the inflamed lungs where they fulfilled their maturation. Neutrophil depletion and PD-L1 blockade during experimental VRI resulted in higher mortality, increased local inflammation, and reduced expression of resolving factors. These findings suggest that PD-L1⁺ neutrophils are important players in disease tolerance by mitigating local inflammation during severe VRI and that they may constitute relevant targets for future immune interventions.

INTRODUCTION

Severe VRI is a clinical condition characterized by the rapid onset of diffuse inflammation in lung parenchyma. Among common respiratory viruses in severe pneumonia are influenza A virus (IAV), influenza B virus, rhinoviruses, and coronaviruses. Viral pneumonia triggers a complex and multifaceted host response involving discrete immune cell populations as well as many inflammatory soluble factors that exert protective or deleterious functions according to the severity and/or the course of infection (1). In worse clinical presentations, pneumonia can progress into life-threatening acute respiratory distress syndrome (ARDS) characterized by a sustained and dysregulated immune response (2, 3). Why are some individuals more or less prone to develop ARDS? A current hypothesis is the advantage of a complex immune trait referred to as “resilience.” This could be defined by the ability of the host to mount a sufficient response to allow pathogen containment/elimination (“resistance”) while preventing over-inflammation and preserving tissue integrity (“tolerance”) (4). During viral ARDS, severe clinical phenotypes are mainly attributable to a defective immune tolerance that can culminate in fatal immunopathology (5).

In this paradigm, neutrophils have been associated with poor prognosis in severe viral pneumonia/ARDS (6), and neutrophil dysfunction has recently emerged as a potential cause of death in severe acute respiratory syndrome coronavirus 2 (SARS-CoV-2) (7–9) and experimental IAV infections (10). These deleterious effects rely on the release of neutrophilic factors such as reactive oxygen species and neutrophil extracellular traps (11–13), which contribute to sustain the local inflammation and tissue damages. In addition, neutrophils can also participate in the resolution of inflammation and tissue healing/regeneration and help in antibody production (14–16). Whether such functional diversity occurs during acute viral infection is unknown.

During viral pneumonia, influx of neutrophils in the lung tissue has been shown to rely on an increased neutrophil egress from the bone marrow (BM), a process referred to as “emergency granulopoiesis” (17), enabling to maintain their presence in inflamed tissues. This “on-demand” mechanism relies on enhanced proliferation of myeloid precursors triggered by soluble factors (e.g., cytokines and/or growth factors) and/or pathogen-associated molecular patterns (17). However, whether these factors can more finely influence neutrophil differentiation/functions remain poorly described during viral pneumonias.

By combining clinical data and experimental IAV-induced severe pneumonia, we identified a subset of regulatory neutrophils characterized by the expression of programmed death-ligand 1 (PD-L1). During viral pneumonia, the emergence of this subset appeared to be remotely imprinted in the BM in an interferon- γ (IFN- γ)-dependent manner before their migration to the inflammatory site. This leads to a transcriptional program associated with regulatory properties. Both neutrophil depletion and PD-L1 blockade heightened susceptibility to experimental viral pneumonia. Thus, our study highlights an important IFN- γ /PD-L1⁺ neutrophil axis serving as a feedback loop to control inflammation during severe viral pneumonia. We

¹INSERM, Centre d'Etude des Pathologies Respiratoires (CEPR), UMR 1100, Tours, France. ²Université de Tours, Faculté de Médecine de Tours, Tours, France. ³Service de Médecine Intensive et Réanimation, CHRU de Tours, Tours, France. ⁴Service de Chirurgie Cardiaque et de Réanimation Chirurgicale Cardio-Vasculaire, CHRU de Tours, Tours, France. ⁵Cytometry and Single-cell Immunobiology Core Facility, University of Tours, Tours, France. ⁶Centre d'Infection et d'Immunité de Lille, Inserm U1019, CNRS UMR 8204, Université de Lille, CHU Lille- Institut Pasteur de Lille, 59000 Lille, France. ⁷Department of Immunology, University of Toronto, Toronto, Ontario M5S 1A8, Canada. ⁸INRAe (Institut National de la Recherche pour l'Agriculture, l'Alimentation et l'Environnement), Université de Tours, ISP, 37380 Nouzilly, France. ⁹Service d'Anatomie et Cytologie Pathologiques, CHRU de Tours, Tours, France.

*Corresponding author. Email: christophe.paget@inserm.fr

†These authors contributed equally to this work.

‡These authors contributed equally to this work.

bring to light an immunological concept in which viral pneumonia remotely controls BM neutrophil differentiation process to assign them with regulatory functions that may pave the way to new therapeutic options in viral pneumonia and ARDS.

RESULTS

PD-L1-expressing neutrophil accumulation correlates with disease severity in patients with severe VRI

To analyze the phenotype of neutrophils during severe VRI, we enrolled 35 patients admitted in intensive care unit for pneumonia/ARDS with diagnosed SARS-CoV-2 ($n = 27$, wild strain) or Flu ($n = 8$, IAV) infections. The baseline characteristics of these patients are presented in Table 1. The proportion of CD10^{low} immature neutrophils (18) was increased in the blood of patients with VRI as compared to healthy donors (Fig. 1, A and B) suggesting an active emergency granulopoiesis. In addition, neutrophils from patients with VRI expressed elevated levels of the inhibitory costimulatory molecule PD-L1 compared to healthy donors (Fig. 1, A and C). Notably, PD-L1 expression could be found on both mature (CD10^{high}) and immature (CD10^{low}) neutrophil subsets (Fig. 1A) with similar proportions (fig. S1A). The concentration of circulating PD-L1⁺ neutrophils was slightly higher in patients with VRI and ARDS as compared to non-ARDS patients (Fig. 1D). The relative proportion of the PD-L1⁺ neutrophils was further increased in endotracheal aspirates (ETA) of intubated patients ($n = 23$) compared to the blood (Fig. 1E) suggesting their accumulation in the airways. Hypoxemia positively correlated with the proportion of airway but not circulating PD-L1⁺ neutrophils (Fig. 1F and fig. S1B). Together, these data suggest that severe VRI is associated with a local and systemic accumulation of PD-L1-expressing neutrophils.

PD-L1⁺ neutrophils accumulate in the lungs during experimental viral pneumonia

To evaluate the biology of lung PD-L1⁺ neutrophils in severe VRI, we infected mice with a highly pathogenic strain of IAV (H3N2 A/Scotland/20/74). In this model, mice die from a deleterious inflammatory response in the lungs despite complete viral clearance (19),

which resembles clinical ARDS. We first assessed the dynamic of airway and parenchyma lung neutrophils during the course of IAV infection. The relative proportion of airway neutrophils rapidly increased upon IAV infection, while it remained unchanged in the lung parenchyma (Fig. 2A, top and middle). However, the absolute number of neutrophils was increased in both compartments to peak at 8 days postinfection (dpi) (Fig. 2A, bottom). Similar to patients with VRI, neutrophils from IAV-infected mice could be segregated based on PD-L1 expression in both airways and parenchyma (Fig. 2B, top). The proportion and absolute number of PD-L1⁺ neutrophils increased as early as 4 dpi (Fig. 2B, middle and bottom) to become the major neutrophil subset during the inflammatory phase (6 to 10 dpi). Notably, neutrophils accounted for ~50% of total PD-L1-expressing leukocytes in airways at 8 dpi (fig. S2) while constituting a minor fraction in the parenchyma (fig. S2). Together, these data demonstrate that PD-L1⁺ neutrophils are a hallmark of the acute phase of experimental IAV infection in the lung.

Lung PD-L1⁺ and PD-L1⁻ neutrophils display discrete transcriptional signatures

To characterize these two neutrophil subsets, we profiled the transcriptomes of PD-L1⁺ and PD-L1⁻ neutrophils isolated from the lungs of IAV-infected mice using single-cell capture using a droplet-based system (Fig. 3A). Following established quality controls and filtering steps (20), 2999 cells (1834 PD-L1⁺ and 1165 PD-L1⁻) were used for downstream analyses. Cell clustering was defined using the Louvain algorithm (21) after merging datasets and reducing dimensionality of the merged dataset through Uniform Manifold Approximation and Projection (UMAP). Analysis of neutrophil marker genes (*S100a9*, *Il1b*, *Dusp1*, and *Lgals3*) confirmed the lineage specificity of our datasets (fig. S3A). We identified five neutrophil clusters (Fig. 3B) with variable prevalence (fig. S3B). PD-L1⁻ neutrophils belonged almost exclusively to clusters 1 and 3 (Fig. 3C and fig. S3C), whereas PD-L1⁺ neutrophils were distributed among clusters 0, 2, and 4 (Fig. 3C and fig. S3C). This suggested substantial transcriptional differences between the two subsets as well as intrasubset heterogeneity (Fig. 3C and table S1).

Table 1. Patients' baseline characteristics at inclusion. IQR, interval quartile range; BMI, body mass index; SAPS2, Simplified Acute Physiology Score 2; SOFA, Sequential Organ Failure Assessment.

	Overall ($n = 35$)	COVID-19 ($n = 27$)	Influenza ($n = 8$)
Age (year), median (IQR)	64 (60; 71)	64 (59; 70)	66 (61; 74)
Male/female, n/n (%)	21/14 (60%)	17/10 (63%)	4/4 (50%)
BMI (kg/m^2), median (IQR)	32 (29; 35)	31 (28; 25)	33 (31; 36)
Type 2 diabetes, n (%)	10 (30%)	8 (30%)	2 (25%)
Hypertension	17 (49%)	13 (48%)	4 (50%)
Chronic respiratory disease, n (%)	1 (3%)	0	1 (13%)
Chronic kidney disease, n (%)	2 (6%)	1 (4%)	1 (13%)
Chronic cardiovascular disease, n (%)	0	0	0
SAPS2, median (IQR)	34 (25; 42)	32 (23; 39)	46 (37; 55)
SOFA at inclusion, median (IQR)	4 (3; 6.5)	4 (2; 6)	8.5 (4; 10)
Invasive mechanical ventilation at inclusion, n (%)	26 (74%)	19 (70%)	7 (88%)

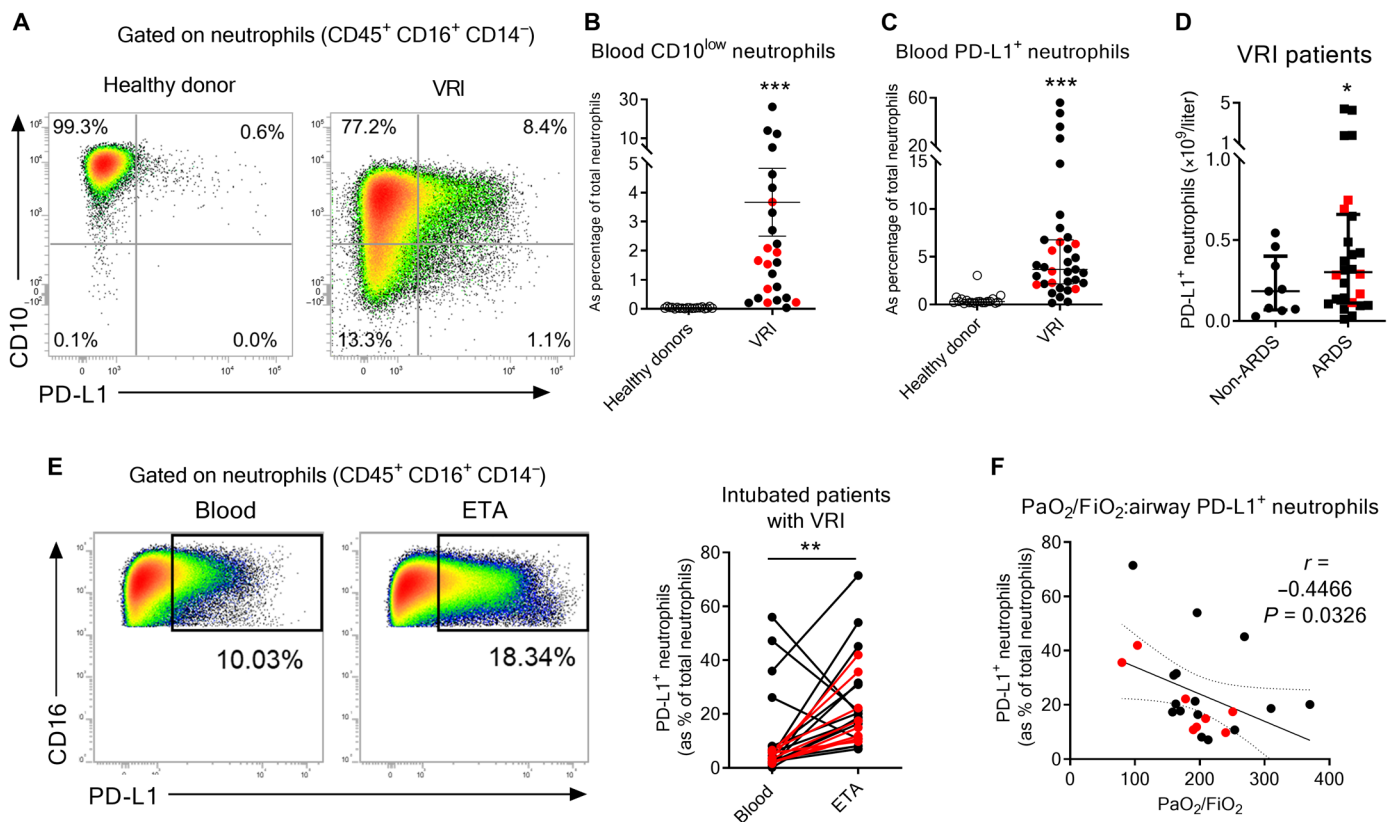


Fig. 1. Neutrophils in patients with severe virus-induced ARDS. (A to D) Flow cytometry analysis of circulating neutrophils in blood of 35 patients with severe viral pneumonia (black dots: COVID-19; red dots: flu) within 48 hours postadmission. (A) Phenotype of circulating neutrophils (CD45⁺ CD3⁻ CD16⁺ CD14⁻). Representative dot plots of CD10 and PD-L1 expression on circulating neutrophils from healthy donors and patients with VRI are shown. [(B) and (C)] Relative proportion of immature CD10^{low} (B) or PD-L1⁺ (C) neutrophils within the total neutrophil compartment in blood of controls and patients. Individual and means \pm SEM are shown ($n = 20$ to 25 per group). (D) Concentration of circulating PD-L1⁺ neutrophils according to the ARDS status. Individual values and means \pm SEM are depicted ($n = 9$ to 26 per group). (E) Representative dot plots of PD-L1 expression on neutrophils from blood or ETA are shown in the left. Paired-analysis of PD-L1⁺ neutrophils in blood and ETA of patients with matched VRI. (F) Spearman's rank correlation of airway PD-L1⁺ neutrophils and hypoxemia levels on admission of intubated patients with viral pneumonia. * $P < 0.05$, ** $P < 0.01$, and *** $P < 0.001$.

To assess further the transcriptional relationships between subsets/clusters, we generated a clustermap using the Pearson's method to order clusters by linkages based on similarity between the correlations (Fig. 3D). Clusters 0, 2, and 4 (PD-L1⁺ neu) were closely related with highest similarities between clusters 0 and 2 (Fig. 3D). Regarding PD-L1⁻ clusters, clusters 1 and 3 appeared to be related albeit with lower correlation than within PD-L1⁺ neutrophil-associated clusters (Fig. 3D).

Comparative analysis of gene expression between the five clusters (Fig. 3E and table S1) indicated that clusters 0, 2, and 4 (PD-L1⁺ neu) shared many differentially expressed genes (DEGs) including genes encoding for major histocompatibility complex class II (MHC-II) (and associated) molecules such as *H2-Aa*, *Cd74*, *H2-Ab1*, *H2-Eb1*, *H2-K1*, and *H2-D1* (Fig. 3E and table S1). Among other notable DEGs, PD-L1⁺ clusters were also defined by high expression of many transcripts encoding for chemokines that have been shown to be released by suppressive tumor-associated neutrophils (22) such as *Ccl2*, *Ccl3*, *Ccl4*, *Ccl5*, *Ccl12*, *Ccl17*, and *Cxcl16* (table S1). Thus, the transcriptomes of PD-L1⁺ neutrophils suggest a specialized subset with regulatory/suppressive functions. PD-L1⁻ neutrophils (clusters 1 and 3) presented several DEGs encoding for

classical markers of neutrophils as *S100a8*, *S100a9*, *Il1b*, *Cxcl2*, *Ccl6*, and *Jund* (Fig. 3E and table S1). Of note, numerous DEGs (*Chil3*, *Retnlg*, *Ngp*, and *Camp*) in clusters 1 and 3 (Fig. 3E and table S1) were reminiscent of differentiating BM neutrophils (20). Moreover, PD-L1⁻ neutrophils preferentially expressed a gene signature of neutrophils with classical antimicrobial (fig. S3D) and phagocytic (fig. S3E) activities.

Clusters 3 (PD-L1⁻) and 4 (PD-L1⁺) were characterized by a high median number of genes, compared to all other clusters (fig. S3F), reminiscent of a strong transcriptional activity associated with cell differentiation and immaturity. In line, these two clusters expressed specific signatures associated with cytoskeleton, gene expression, and cell cycle (fig. S3G).

This analysis reveals that PD-L1⁻ and PD-L1⁺ neutrophils have distinct transcriptional signatures during IAV infection, which are evocative of classical inflammatory and regulatory/suppressive functions, respectively.

PD-L1⁺ neutrophils are immature and apoptosis resistant

To evaluate their level of maturation, we first performed microscopy-based morphological analysis on isolated lung neutrophil subsets

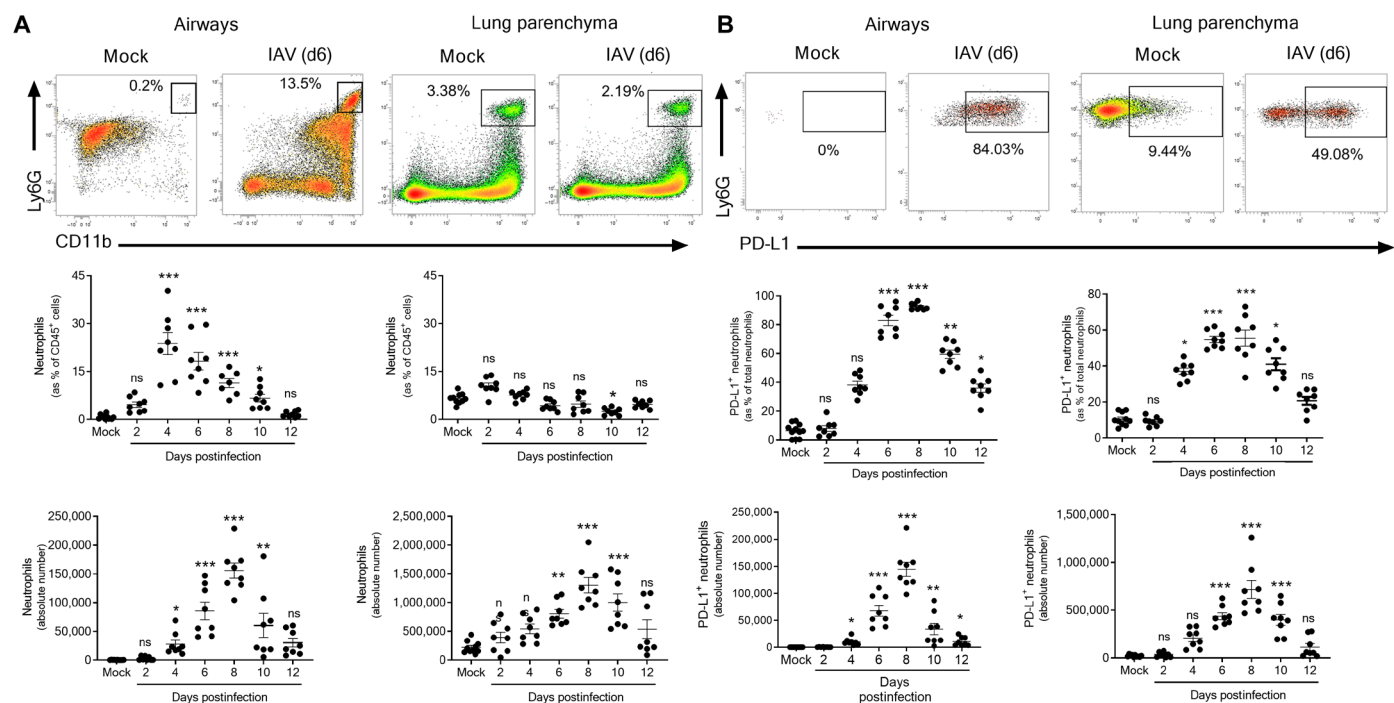


Fig. 2. Dynamics and phenotype of neutrophils during experimental IAV infection. Wild-type (WT) C57BL/6j mice were intranasally infected with mock or IAV [150 plaque-forming units (PFU)] A/H3N2/Scotland/20/74 strain. Mice were euthanized at indicated time points, and BAL and lungs were harvested. **(A)** Relative proportion and absolute numbers of neutrophils in airways and lung parenchyma were evaluated by flow cytometry. Representative dot plots of neutrophils in airway and lung parenchyma from mock and IAV-infected mice (6 dpi) are shown in the top. Individual and means \pm SEM pooled from three independent experiments are shown in the bottom (8 to 10 mice per group). **(B)** Relative proportion and absolute numbers of PD-L1⁺ neutrophils in airways and lung parenchyma were evaluated by flow cytometry. Representative dot plots of PD-L1⁺ neutrophils in airway and lung parenchyma from mock and IAV-infected mice (6 dpi) are shown in the top. Individual and means \pm SEM pooled from three independent experiments are shown in the bottom (8 to 10 mice per group). ns, not significant; * $P < 0.05$, ** $P < 0.01$, and *** $P < 0.001$.

from IAV-infected mice. The PD-L1⁺ fraction was enriched for metamyelocytes and banded neutrophils, whereas the PD-L1⁻ fraction contained a vast majority of classical mature neutrophils with uniform morphology (Fig. 4A). Higher prevalence of immature stages within the PD-L1⁺ fraction could also be illustrated based on CD101 expression (Fig. 4B) (23). In addition, a large proportion of PD-L1⁺ neutrophils from IAV-infected mice were FSC^{high} (fig. S4A), which is reminiscent of an immature phenotype (24). The presence of immature stages in the PD-L1⁺ subset could also be illustrated by the higher proportion of Ki67⁺ cells (Fig. 4C) as well as a higher transcriptional G₂M cell cycle score in PD-L1⁺ neutrophil-associated clusters (fig. S4B). To finely map the maturation stages at the transcriptional level, we adapted to our datasets the “neutrotime” signature (20), a model that enables to project neutrophils onto a single maturation ordering from BM precursors to mature neutrophils in peripheral tissues under normal and inflamed conditions. We took advantage of a published gene set (23) to identify neutrophil precursors within our dataset. A module score for each cell was calculated and revealed a high expression of the precursor signature in cluster 3 (fig. S4C). Thus, we calculated a pseudotime (25) using cluster 3 as a root (fig. S4D). The linear ordering of neutrophils according to the maturation score indicated that cluster 4 comprised immature cells (Fig. 4D). Regarding other PD-L1⁺ clusters, the model suggested that cluster 0 was less mature than cluster 2 (Fig. 4D). The cluster 1 that encompasses the vast majority of PD-L1⁻ neutrophils emerged as the most mature subset within our dataset (Fig. 4D).

In parallel, we also interrogated the potential differential apoptotic profile of the two neutrophil subsets in IAV-infected mice. On the basis of propidium iodide/annexin V staining, classical neutrophils expressed a marked phenotype of late-apoptotic cells compared to the regulatory subset (Fig. 4E). In line, the neutrophil transcriptomes confirmed an enrichment for genes associated with negative execution of apoptosis in PD-L1⁺ clusters (fig. S4E). However, this signature was also enriched in cells of cluster 3 in agreement with their immature profile (fig. S4E). Moreover, PD-L1⁺ neutrophil-associated clusters displayed increased expression of *Cd47* (fig. S4F), a “do not eat me” signal that may confer resistance to efferocytosis (26). Together, lung PD-L1⁺ neutrophils from IAV-infected mice displayed multiple features of immature cells and higher resistance to apoptosis.

IAV-induced lung PD-L1⁺ neutrophils have regulatory functions

We evaluated the phenotype and functions of lung PD-L1⁺ neutrophils from IAV-infected mice. In line with the expression of numerous genes encoding for MHC-II molecules (Fig. 3E and table S1), we confirmed by flow cytometry that lung PD-L1⁺ neutrophils from IAV-infected mice expressed high levels of MHC-II as compared to their PD-L1⁻ counterparts (Fig. 5A). We also tested two gene sets from Gene Ontology (GO) associated with the regulation of the inflammatory response on the transcriptomes. We observed a high signature for “positive regulation of the inflammatory response” in mature PD-L1⁻ neutrophils (cluster 1), while featured

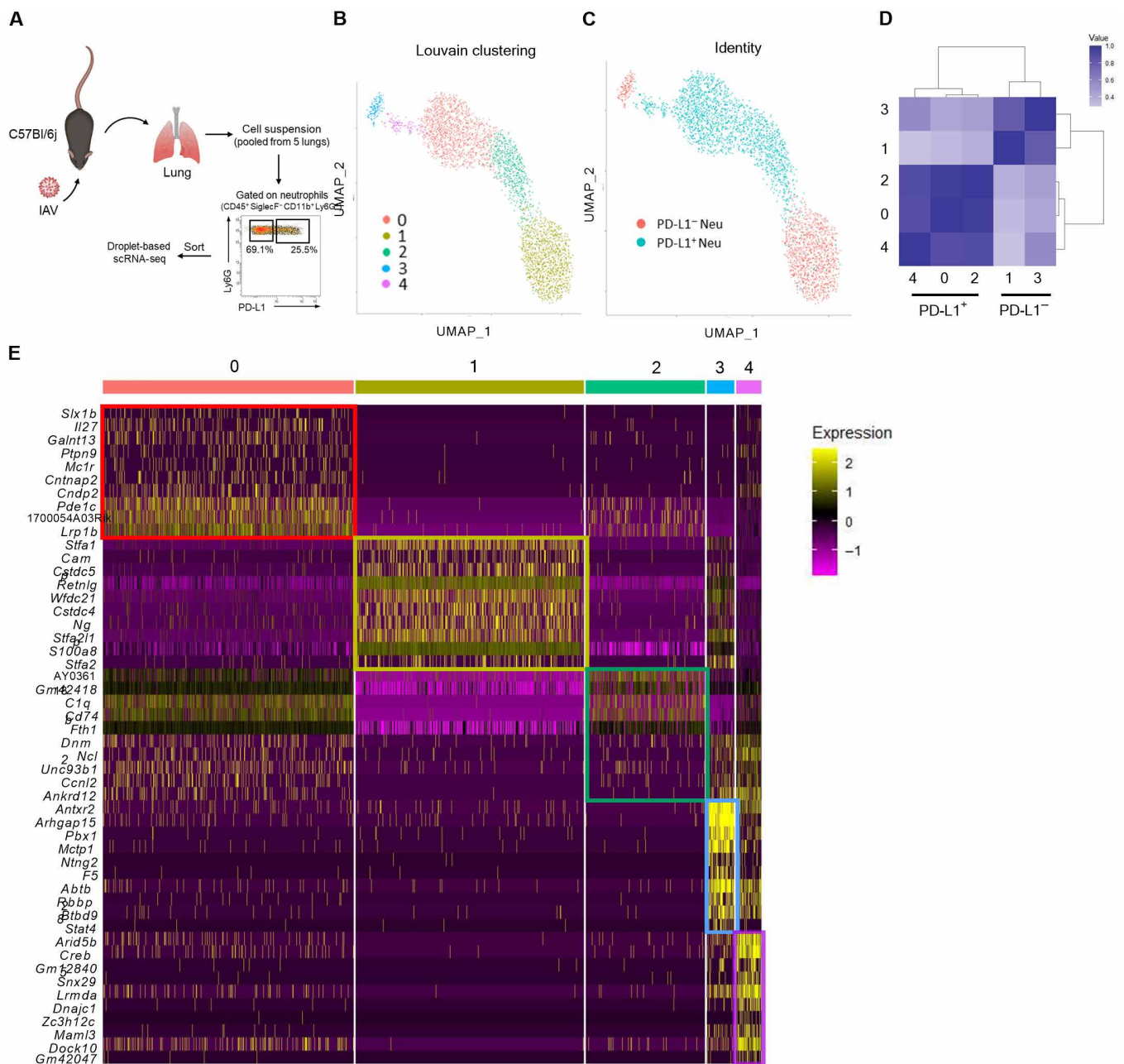


Fig. 3. Single-cell RNA sequencing profiling of lung neutrophil subsets from IAV-infected mice. (A to E) WT C57BL/6j mice were intranasally instilled with IAV (150 PFU) A/H3N2/Scotland/20/74 strain and euthanized at day 11. Lungs were collected and processed before neutrophil sorting based on PD-L1 expression. (A) Representation of the experimental workflow used to generate single-cell RNA sequencing (scRNA-seq) data. (B) Identification of cell clusters using the graph-based Louvain algorithm (resolution = 0.5) on UMAP. Each dot represents one cell (2999 cells). (C) Identity of PD-L1⁺ and PD-L1⁻ neutrophils projected on the UMAP. (D) Clustermap of neutrophil subsets comparing each pair of clusters using the Pearson's correlation with hierarchical clustering. (E) Expression of the top 10 marker genes for each cluster identified in (B).

genes for “negative regulation of the inflammatory response” were enriched in PD-L1⁺ neutrophil-associated clusters especially the cluster 2 (Fig. 5B).

To directly assess the functions of PD-L1⁻ and PD-L1⁺ neutrophils, we first analyzed their production of arginase-1 (Arg-1), a key effector in the regulation of inflammation, which suppresses T cell function (27). *Arg1* transcripts could be detected in a substantial

proportion of cells belonging to PD-L1⁺ neutrophil clusters (fig. S5). Moreover, lung PD-L1⁺ neutrophils produced high amounts of Arg-1 during the course of infection, while PD-L1⁻ neutrophils failed to do so (Fig. 5C). Of note, PD-L1⁺ neutrophils displayed a higher capacity to produce Arg-1 during the resolution phase (Fig. 5C). Conversely, PD-L1⁺ neutrophils produced less myeloperoxidase (Fig. 5D) and oxidants (Fig. 5E) than PD-L1⁻ neutrophils.

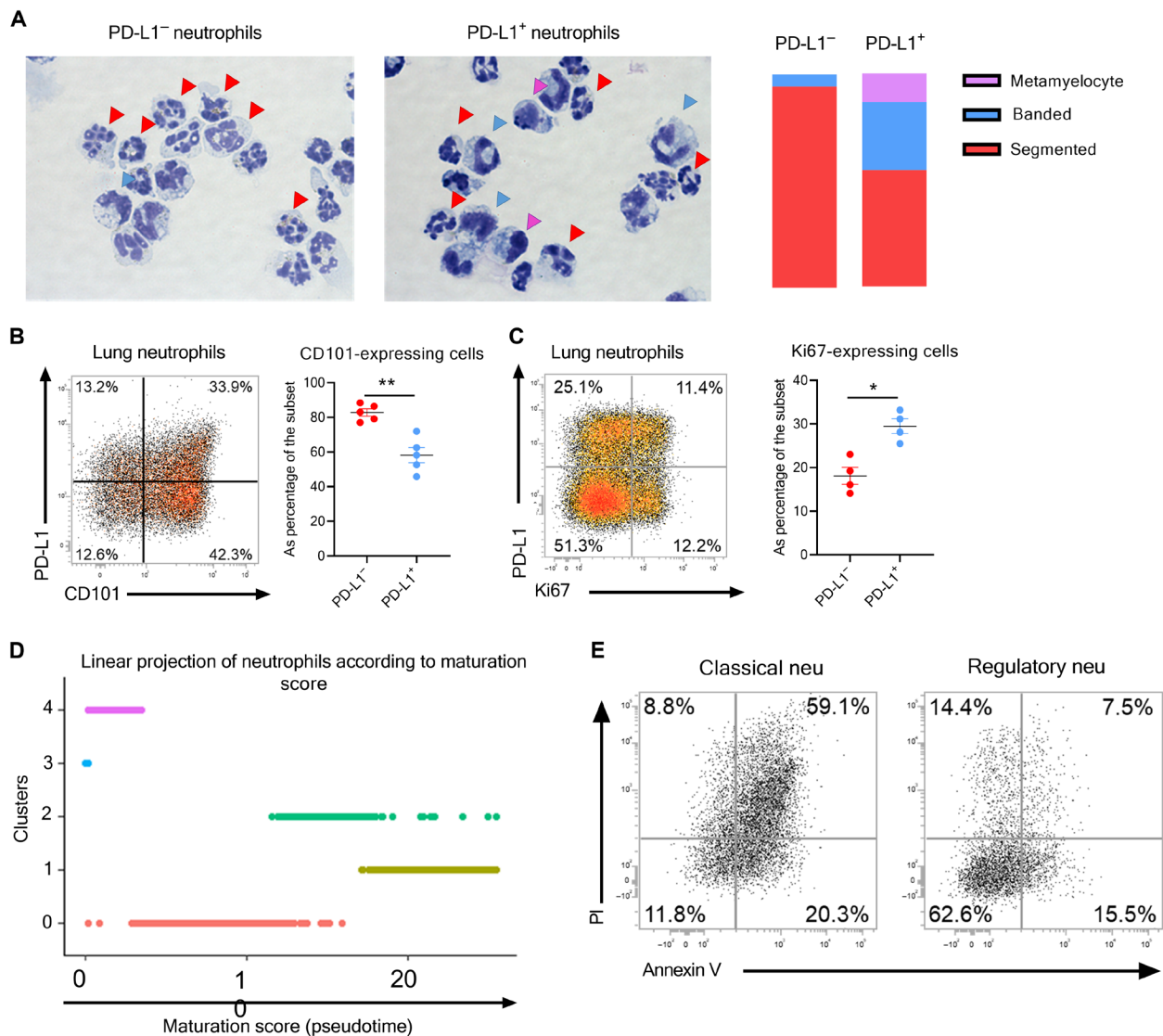


Fig. 4. Morphology, maturation, and life span of lung neutrophilic subsets in IAV-infected mice. (A to E) WT C57BL/6j mice were intranasally instilled with mock or IAV (150 PFU) A/H3N2/Scotland/20/74 strain. Mice were euthanized, and the whole lungs were collected at 7 dpi. (A) Representative light microscopy pictures of cytopsin of purified lung neutrophil subsets. Neutrophil developmental stages were defined on the basis of morphology and depicted in the right ($n = 3$); $\times 200$, original magnification. [(B) and (C)] Representative dot plots of CD101 (B) or Ki67 (C) expression on lung neutrophils from IAV-infected mice based on PD-L1 expression. Relative proportions of CD101- (B) or Ki67-expressing (C) cells per subset are shown in the right. Individual values and means \pm SEM from two independent experiments (four to five mice per group) are shown. (D) Linear projection of cells according to pseudotime score from Monocle3 according to cluster identities. (E) Apoptotic profile of lung neutrophil subsets from IAV-infected mice. A representative dot plot of two independent experiments for both subsets is shown (six mice per group). PI, propidium iodide.

The potential suppressive activities of PD-L1⁺ neutrophils were then evaluated on activated T cells. Addition of purified neutrophils from airways of IAV-infected mice (containing 90% of PD-L1⁺ neutrophils (Fig. 2B) reduced the proliferative capacities of both CD4⁺ and CD8⁺ T cells in a ratio-dependent manner (Fig. 5F). T cell proliferation could be rescued upon PD-L1 blockade (Fig. 5F). Together, these data demonstrate that PD-L1⁺ neutrophils that emerge during IAV infection have regulatory/suppressive functions.

PD-L1⁺ neutrophils are readily detectable in the BM during IAV infection and preferentially migrate toward the lungs

Our data suggested that IAV infection triggers the egress of BM neutrophils containing immature cells (Figs. 3E and 4B). We found that

the proportion of BM neutrophils rapidly decreased starting at day 4 post-IAV infection (Fig. 6A, left). Although only a minute fraction of PD-L1⁺ neutrophils could be detected in the BM of naive mice, this subset increased as soon as 4 dpi (Fig. 6A, right). BM PD-L1⁺ neutrophils from IAV-infected mice also readily expressed MHC-II (fig. S6A). Consistent with a rapid mobilization of BM neutrophils, the relative proportion of neutrophils increased in the blood of IAV-infected mice (Fig. 6B, left). Moreover, this was also accompanied with an increase in the proportion of circulating PD-L1⁺ neutrophils (Fig. 6B, right). In addition, BM and blood PD-L1⁺ neutrophils preferentially expressed CD49d (Fig. 6C), a key integrin in the homing of neutrophils in the lung tissue upon infection (28). Higher levels of CD49d were also detected on lung PD-L1⁺ neutrophils as

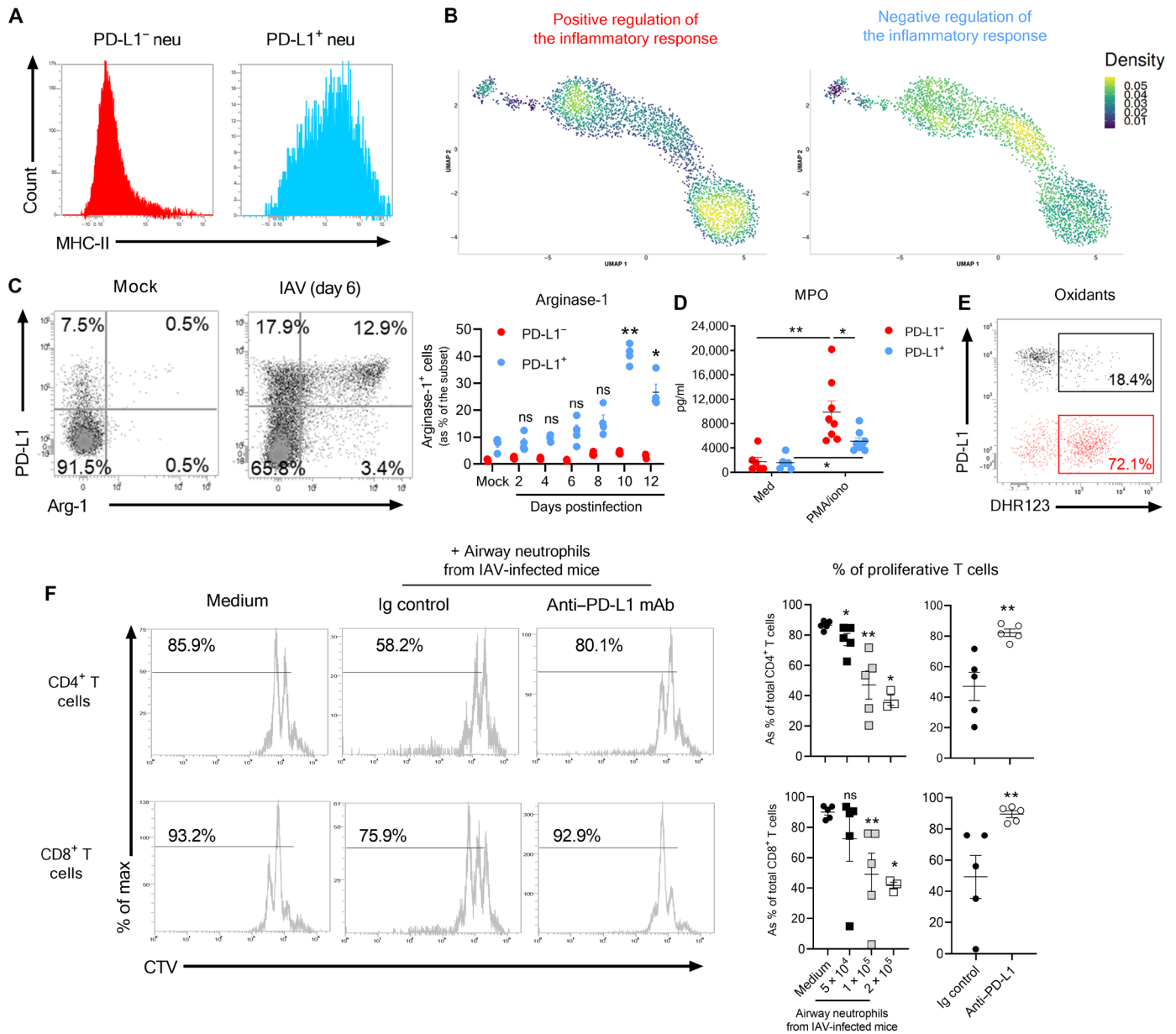


Fig. 5. Phenotype and regulatory functions of lung PD-L1⁺ neutrophils. WT C57BL/6j mice were intranasally instilled with mock or IAV (150 PFU) A/H3N2/Scotland/20/74 strain. Mice were euthanized, and the whole lungs were collected at indicated time points. **(A)** Expression of MHC-II on lung neutrophils from IAV-infected mice (7 dpi) was evaluated by flow cytometry. Representative dot plots according to neutrophilic subset is shown. **(B)** Density plot of “positive” and “negative” regulation of the inflammatory response. **(C)** Relative proportion of Arg-1-producing neutrophils according to subset and time course of infection. Representative dot plots are shown in the left. Individual values and means ± SEM from two independent experiments (four mice per group per time point) are shown in the right. **(D)** Levels of MPO produced ex vivo by purified neutrophil subsets (7 dpi) upon short-term PMA stimulation. Individual values and means ± SEM from two independent experiments are shown. **(E)** Levels of oxidants in neutrophil subsets (7 dpi) measured 5 min after incubation with DHR123. Representative dot plots from one experiment of two are shown. **P* < 0.05 and ***P* < 0.01. **(F)** PD-L1-mediated suppressive effect of neutrophils from IAV-infected mice (8 dpi) on T cell proliferation. CTV-stained spleen cells from naive mice were cultured with plate-bound anti-CD3 mAbs with or without indicated numbers of neutrophils from IAV-infected mice in the presence of either Ig control or anti-PD-L1 mAb. Proliferation of CD4⁺ and CD8⁺ T cells was monitored after 72 hours based on CTV dilution. Representative dot plots showing CTV expression in CD4⁺ (top) and CD8⁺ (bottom) T cells are shown in the left. Individual values and means ± SEM of proliferation rate from two independent experiments are depicted in the right. **P* < 0.05 and ***P* < 0.01.

Downloaded from https://www.science.org at INRAE Institut National de la Recherche Agronomique et de l'Environnement on October 17, 2024

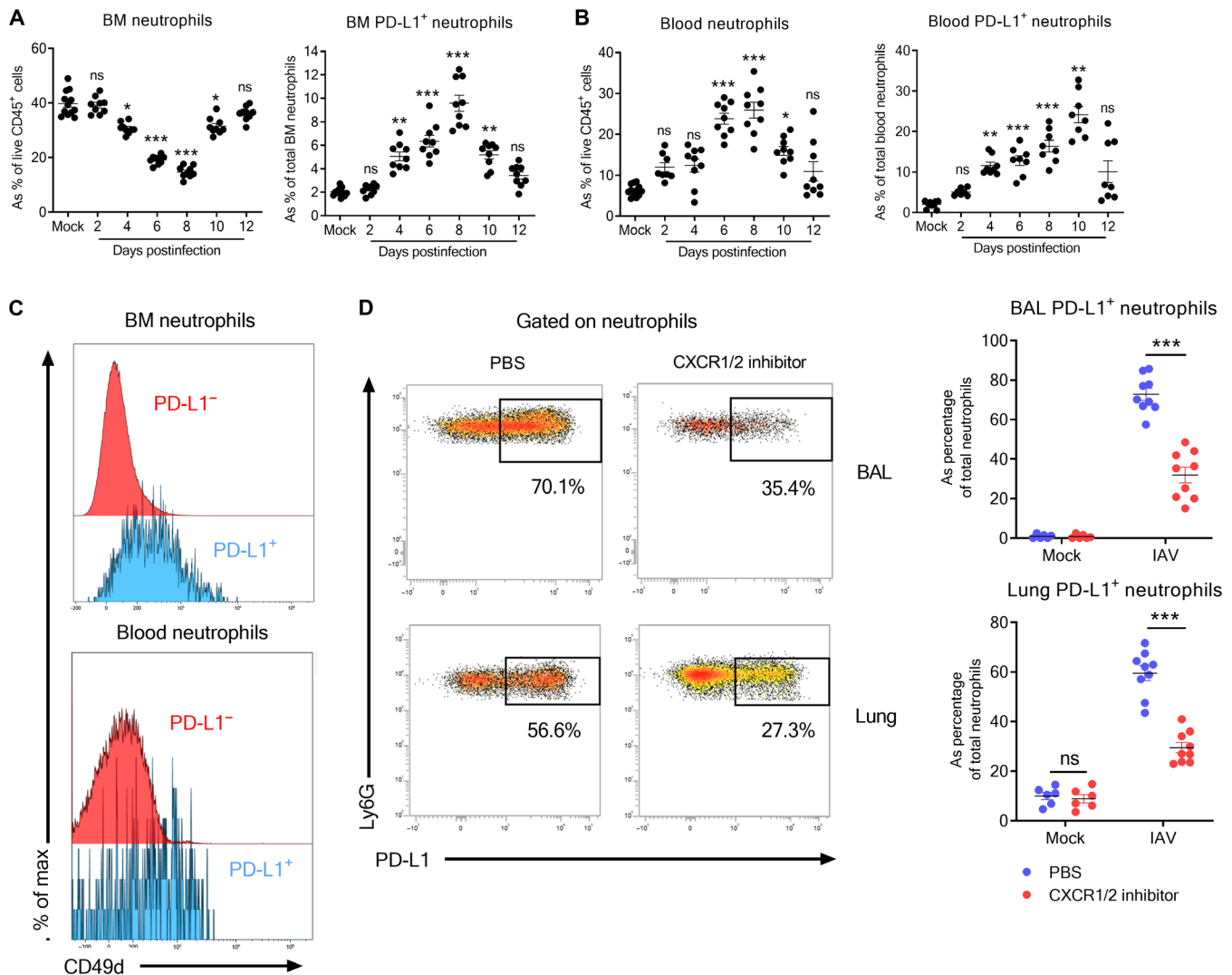


Fig. 6. BM origin of IAV-induced PD-L1⁺ neutrophils. WT C57BL/6j mice were intranasally infected with IAV (150 PFU) A/H3N2/Scotland/20/74 strain. Mice were euthanized at indicated time points. **(A)** Relative proportion of neutrophils (subsets) in BM of IAV-infected mice was evaluated by flow cytometry. Individuals and means \pm SEM from three independent experiments are shown (8 to 12 mice per group). **(B)** Frequency of circulating neutrophils (subsets) of IAV-infected mice was evaluated by flow cytometry. Individuals and means \pm SEM from three independent experiments are shown (7 to 12 mice per group). **(C)** Expression of CD49d on neutrophil subsets from IAV-infected mice (7 dpi) according to PD-L1 expression. Representative histograms of BM (top) and blood (bottom) neutrophilic subsets are shown. **(D)** Effect of CXCR1/2 inhibition on lung PD-L1⁺ neutrophils in IAV-infected mice. Representative dot plots of PD-L1⁺ cells within the BAL (top) and lung parenchyma (bottom) neutrophil pool from IAV-infected mice treated or not with CXCR1/2 inhibitor are represented in the left. Individuals and means \pm SEM from two independent experiments are shown (six to nine mice per group) in the right. * $P < 0.05$, ** $P < 0.01$, and *** $P < 0.001$.

compared to their PD-L1⁻ counterpart (fig. S6B). In addition to its anti-apoptotic signals, *Cd47*, which expression is increased in lung PD-L1⁺ neutrophil-associated clusters (fig. S4F), supports the migration of neutrophils to the site of infection (29). Consistent with a preferential migration of BM PD-L1⁺ neutrophils toward the lung, no enrichment was observed in other peripheral organs of IAV-infected mice such as spleen and liver (fig. S6C), although we noticed a high proportion of PD-L1⁺ neutrophils in the liver of naive mice (fig. S6D).

Neutrophil migration from the lung is known to be dependent on CXCR2 (30). Upon CXCR2 blockade (31), the frequency of lung neutrophils was decreased at 6 dpi (fig. S6E). This effect was even more pronounced on the PD-L1⁺ subset (Fig. 6D). As expected, this

treatment led to an accumulation of neutrophils in the BM (fig. S6E), which was more marked on PD-L1-expressing neutrophils (fig. S6F). Overall, BM PD-L1⁺ neutrophils are quickly mobilized into the lungs during IAV infection.

IAV-induced IFN- γ programs BM neutrophils for regulatory functions

The emergence of PD-L1⁺ neutrophils in the BM in the early stages of IAV infection suggests that they acquire their regulatory functions during their differentiation and maturation within the BM. First, we interrogated whether the IAV infection influenced the ability of BM hematopoietic stem cells (HSC) to generate neutrophils. Thus, BM HSC from either naive or IAV-infected mice were differentiated

in vitro into BM-derived neutrophils (BMN). In this setting, both precursors generated the same amount of BMN (Fig. 7A) with ~20% of these latter expressing PD-L1 (Fig. 7A).

BM PD-L1⁺ neutrophils from IAV-infected mice preferentially coexpressed Sca-1 (Ly6A/E) (Fig. 7B), a common IFN-stimulated gene (32). In parallel, we detected an increased number of transcripts encoding for IFN- γ in the BM samples of IAV-infected mice as soon as 2 dpi (fig. S7A), which precedes the emergence of PD-L1⁺ neutrophils. Moreover, BM PD-L1⁺ neutrophils from IAV-infected

mice preferentially coexpressed IFN- γ R1 (CD119) (Fig. 7C). Thus, we differentiated BM precursors from naive mice into BMN in the presence of recombinant mouse IFN- γ (rmIFN- γ). Addition of IFN- γ culminated in the generation of more than 90% of PD-L1⁺ BMN (Fig. 7D) coexpressing Sca-1 and MHC-II (fig. S7B), an effect that was abrogated using *Ifngr*^{-/-} BM precursors (fig. S7C). Moreover, PD-L1⁺ BMN produced Arg-1 but only in the presence of rmIFN- γ (Fig. 7E). Acquisition of the regulatory phenotype was optimal under sustained pressure of IFN- γ (fig. S7D). Notably, the use

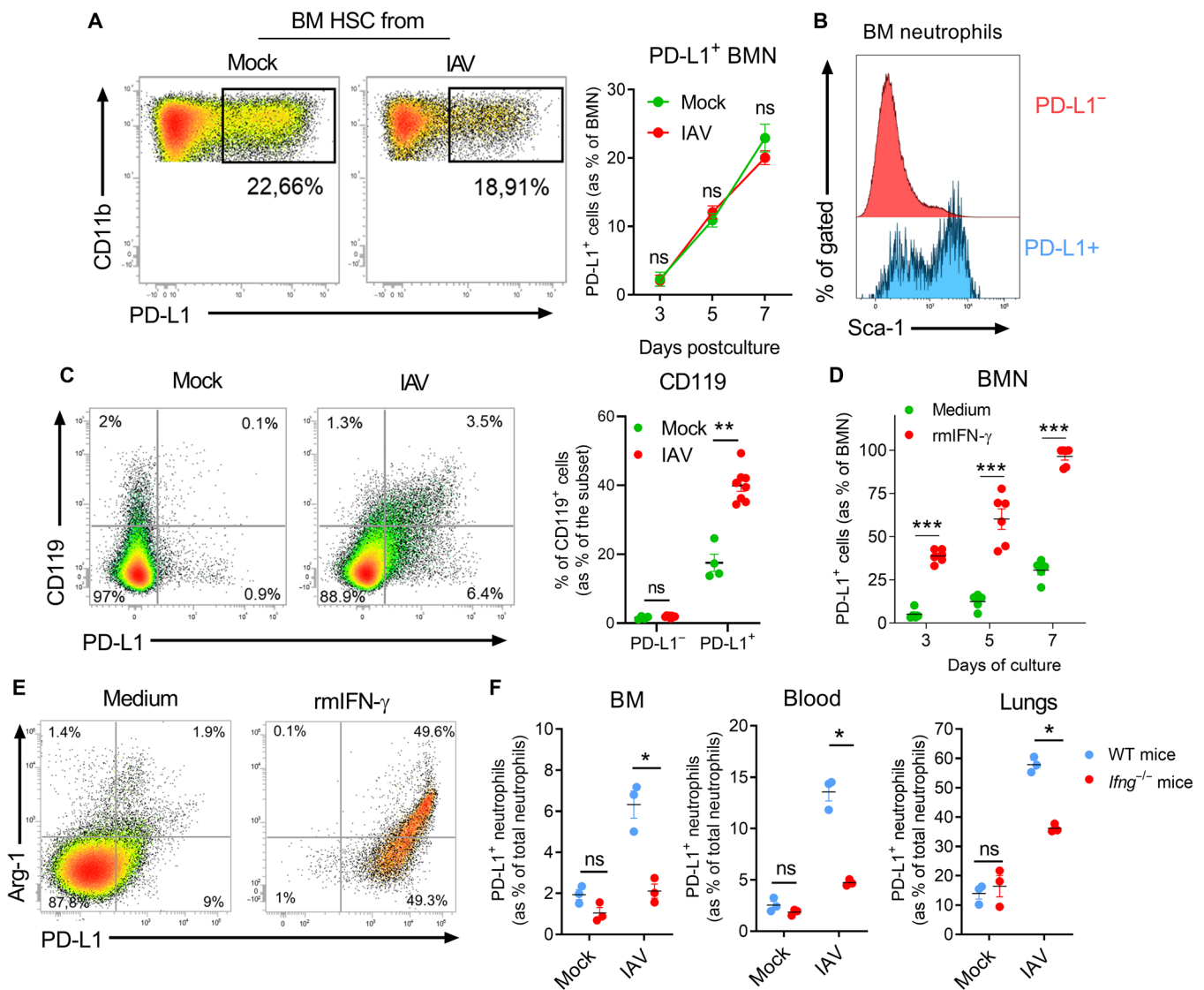


Fig. 7. IFN- γ primes BM neutrophils for regulatory functions. (A) Representative dot plots of the relative proportion of PD-L1⁺ BMN (within total BMN: CD11b⁺ Ly6G⁺) differentiated from stem cells isolated from BM of mock-treated or IAV-infected mice (7 dpi) are shown. Means \pm SEM at indicated time points from two independent experiments are shown in the right. (B) Representative histograms of Sca-1 expression on BM neutrophil subsets from IAV-infected mice (7 dpi). (C) Expression of CD119 on BM neutrophils according to PD-L1 expression in naive and IAV-infected mice (7 dpi) was evaluated by flow cytometry. Representative dot plots are shown in the left. Individuals and means \pm SEM of CD119 expression according to neutrophil subset from two independent experiments are shown (four to eight mice per group) in the right. (D) Relative proportions of PD-L1⁺ BMN (within total BMN) differentiated from BM stem cells isolated from naive mice during the course of differentiation in the presence of medium or recombinant mIFN- γ . Individuals and means \pm SEM at indicated time points from three independent experiments are shown. (E) Expression of Arg-1 by BMN subsets differentiated in the presence or not of rmIFN- γ . Representative dot plots from two independent experiments are shown. (F) Relative proportion of PD-L1⁺ neutrophils in various tissues of mock or IAV-infected mice (7 dpi) from WT and *Ifng*^{-/-} mice. Individual values and means \pm SEM are shown (three mice per group). * P < 0.05, ** P < 0.01, and *** P < 0.001.

of rmIFN- γ significantly decreased the absolute number of generated BMN as compared to controls (fig. S7E). This was not associated to a higher mortality (Fig. S7F) but to a lower proliferative rate upon rmIFN- γ pressure (fig. S7G) as compared to differentiating PD-L1⁻ BMN. However, this reflected a higher capacity of the PD-L1⁻ subset to cycle as compared to PD-L1⁺ BMN independently of rmIFN- γ usage (fig. S7H) at least under in vitro setting. Of note, transcriptomic data also pointed to an early effect of IFN- γ on developing neutrophils since an IFN- γ -mediated signaling pathway signature was enriched in immature lung neutrophil clusters (fig. S7I). Consistent with a role for IFN- γ in the generation of PD-L1⁺ regulatory neutrophils, this signature was also enriched in clusters 0 and 4 as compared to cluster 1 (fig. S7J).

To evaluate the role of IFN- γ in vivo, BM PD-L1⁺ neutrophils were analyzed in IAV-infected *Ifng*^{-/-} mice. As compared to control mice, a decrease in the number of neutrophils was noted in lungs of *Ifng*^{-/-} mice (fig. S7J). Conversely, neutrophil numbers were increased in the blood of *Ifng*^{-/-} mice (fig. S7J). Analysis of neutrophil subsets indicated that the PD-L1⁺ fraction was the most affected subset upon IFN- γ deficiency in all compartments (Fig. 7F). Moreover, the remaining PD-L1⁺ neutrophils from *Ifng*^{-/-} mice coexpressed lower levels of Sca-1 and MHC-II as compared to their wild-type counterparts (fig. S7K). Overall, IAV infection-dependent IFN- γ primes developing neutrophils in the BM resulting in emergence of PD-L1⁺ neutrophils with a regulatory phenotype.

Presence of PD-L1⁺ neutrophils is associated with protection during IAV infection

Neutrophils have been largely described as deleterious cells in experimental models of IAV infection (10, 13, 33). By starting neutrophil depletion on 4 dpi, a time point that corresponds to the emergence of PD-L1⁺ neutrophils in the lungs, we observed an increased mortality of IAV-infected mice as compared to controls (Fig. 8A). This treatment was not associated with a reduced viral clearance as compared to controls (fig. S8A). However, at 8 dpi, we detected increased levels of soluble inflammatory mediators [IFN- γ , interleukin-1 β , and tumor necrosis factor- α (TNF- α)] (Fig. 8B). CCR2-expressing myeloid cells including monocyte-derived dendritic cells (MoDC) and inflammatory monocytes have been associated to immunopathology during IAV infection (34–36). A higher infiltration of MoDC and inflammatory monocytes in the lung tissue could be observed in neutrophil-depleted mice (Fig. 8C and fig. S8B). A higher activation status of the CD8⁺ T and natural killer cells that can contribute to immunopathology in highly virulent IAV models (37, 38) was also noted (fig. S8C). This was accompanied by a reduced number of alveolar macrophages (AM) (Fig. 8C), which contribute to tissue repair during IAV infection (39, 40). No change was observed for total conventional DC (Fig. 8C and fig. S8B). Histological analysis of hematoxylin and eosin (H&E)-stained lung sections confirmed the increased lesions of pneumopathy in neutrophil-depleted mice as illustrated by increased edema, increased alveolar septal thickening, and fibrin debris (fig. S8D).

As a complementary approach, IAV-infected mice were treated with a neutralizing anti-PD-L1 monoclonal antibody (mAb; 10F.9G2) starting at 4 dpi (Fig. 8D). In this setting, PD-L1 blockade also did not affect viral clearance (fig. S8E) and led to higher local inflammation as judged by levels of inflammatory cytokines (Fig. 8E). PD-L1 neutralization led to an accumulation of MoDC and inflammatory monocytes (Fig. 8F). In addition, we observed a higher infiltration of PD-L1⁻ “classical” neutrophils upon this treatment (Fig. 8F). Again, this was

paralleled with a significant decrease in AM absolute number (Fig. 8F). Moreover, we compared the transcriptional inflammatory signature of the lungs from control and anti-PD-L1-treated mice based on 30 selected genes encoding for proteins involved in IAV-related immune regulation. Unsupervised hierarchical clustering indicated the existence of three modules that could discriminate the two groups (Fig. 8G). In the lung of anti-PD-L1-treated mice, we noticed a reduced expression of genes encoding for factors associated with resolution of inflammation and tissue healing in IAV-induced pneumonia (module 2) as compared to controls such as *Areg* (41), *Igf1* (42), *Csf2* (43), *Tgfb1* (44), *Ptges2* (45), and *Il17rb* (46), as well as genes encoding for angiogenic factors (*Vegfa*) (Fig. 8H) (47). Conversely, module 1 comprised up-regulated transcripts in PD-L1-treated mice for proinflammatory genes (e.g., *Ccl2*, *Ifng*, and *Il13*) associated with deleterious IAV-mediated host response (Fig. 8H) (48–50). Together, our findings suggest that PD-L1⁺ lung neutrophils control the deleterious inflammatory response associated with IAV infection.

DISCUSSION

Here, we demonstrated that lung viral infection led to the rapid emergence of regulatory PD-L1-expressing neutrophils within the BM in an IFN- γ -dependent manner and can be observed before their migration toward the inflamed/damaged tissue. In line with the literature (7), we could detect PD-L1⁺ neutrophils in the blood of patients with severe VRI. Here, we also bring evidence for their high prevalence in airways of matched patients. VRI-associated PD-L1⁺ neutrophils were previously defined as “dysfunctional” with impaired antimicrobial activity (7). Although they could be considered dysfunctional in regards to classical neutrophils, our data rather support that PD-L1⁺ neutrophils acquire a specific functional program associated with regulatory properties. While PD-L1⁺ neutrophils appear to exert a protective role in severe experimental VRI by limiting local inflammatory response, the situation in clinics is likely much more complex. Bacterial co-/super-infections often worsened the clinical picture during VRI (51), and the emergence of regulatory neutrophils might also be at the expense of an optimal antimicrobial response (16) and therefore might pave the way for these infections. Thus, this study identifies a pivotal, but sensitive, axis in the resistance/tolerance balance during severe viral pneumonia/ARDS. In clinics, neutrophils are still analyzed as a homogeneous cell population, and further studies should be encouraged to better define the neutrophilic phenotype in relation to endotypes.

Excessive activation of proinflammatory neutrophils has been shown to contribute in VRI-induced lethality (6). However, several studies reported that neutrophil depletion led to various outcomes in VRI-induced lethality. These discrepancies likely stem from differences in neutrophil depletion regimen (doses of mAb and time of depletion), acuteness of the model (sublethal versus lethal), and the strain of virus used (10, 52–54). Our data indicate that these differences may also arise from the existence of neutrophilic subsets with opposite functions. Whether the models of VRI influence the emergence and/or the magnitude of regulatory PD-L1⁺ neutrophils will deserve further investigations.

Both functional and transcriptomic analyses indicate that VRI-induced lung PD-L1⁺ neutrophils display functional properties associated with negative regulation of inflammation including PD-L1-mediated control of T cells, Arg-1 production, and reduced capacity to produce classical inflammatory mediators. Understanding

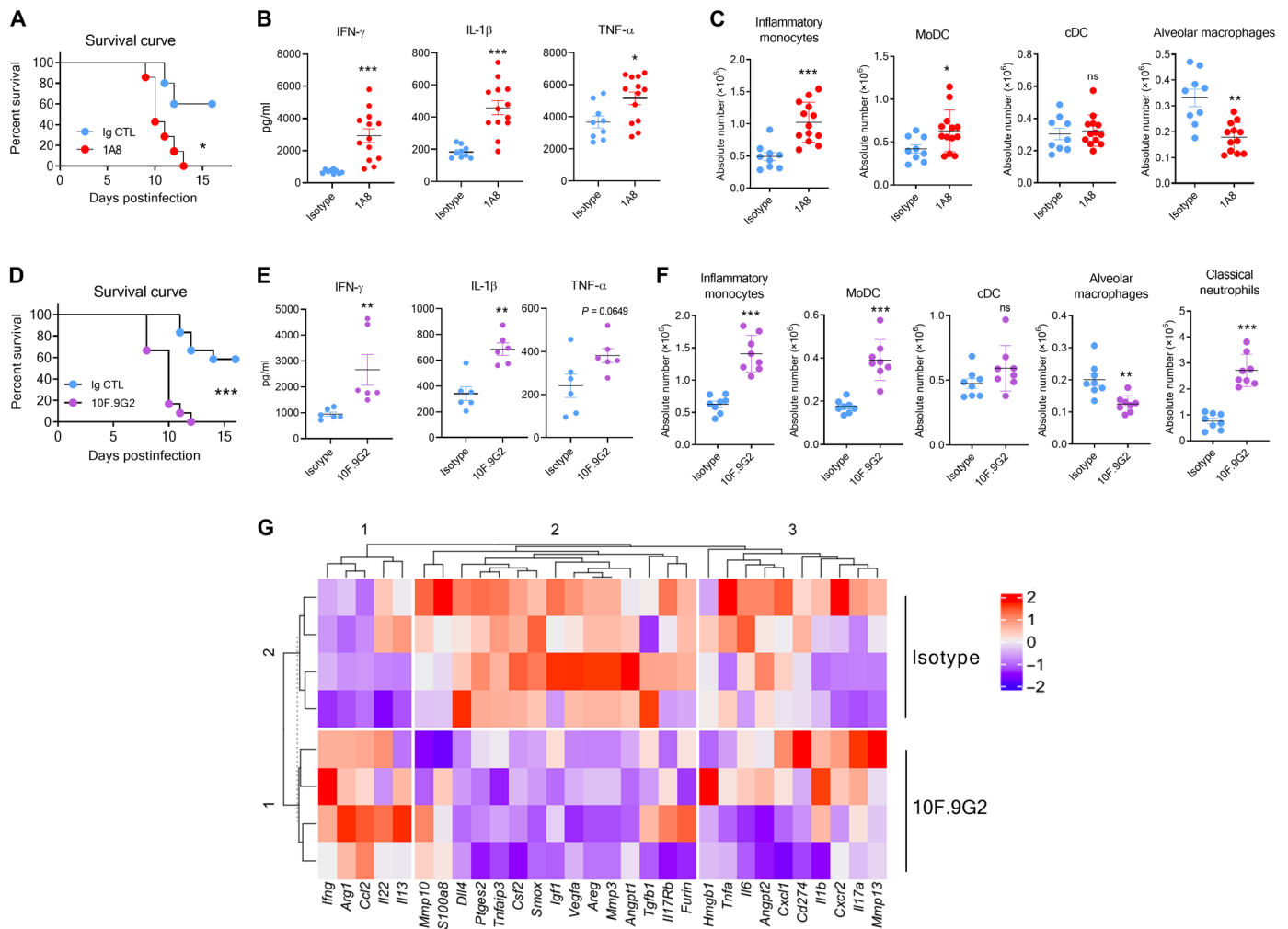


Fig. 8. Neutrophil depletion or PD-L1 blockade influence mouse survival and inflammatory response during IAV infection. (A to G) WT C57BL/6j mice were intranasally infected with IAV (150 PFU) A/H3N2/Scotland/20/1974 strain. Mice were treated from 4 dpi and every second day with isotype control or 1A8. (A) Survival was monitored daily (five to seven mice per group). (B) Mice were euthanized on day 8, and lungs were collected. Individuals and means \pm SEM of IFN- γ , IL- β , and TNF- α levels in lung homogenates of isotype- or 1A8-treated IAV-infected mice from two independent experiments are shown (9 to 13 mice per group). (C) Individual values and means \pm SEM of inflammatory monocytes, monocyte-derived DC, conventional DC, and AM from two independent experiments are shown (9 to 13 mice per group). [(D) to (G)] from 4 dpi and every second day with isotype control or anti-PD-L1 mAb. (D) Survival was monitored daily (12 mice per group). [(E) to (G)] Mice were euthanized on day 8, and lungs were collected. (E) Individuals and means \pm SEM of IFN- γ , IL- β , and TNF- α levels in lung homogenates of isotype- or anti-PD-L1-treated IAV-infected mice from two independent experiments are shown (six mice per group). (F) Individual values and means \pm SEM of inflammatory monocytes, monocyte-derived DC, conventional DC, AM, and classical neutrophils from two independent experiments are shown (eight mice per group). (G) Unsupervised hierarchical clustering of the 30 genes imputed from transcriptional analysis of individual samples ($n = 4$ per group). * $P < 0.05$, ** $P < 0.01$, and *** $P < 0.001$.

the precise mechanisms involved in their protective in vivo effect is now under investigation.

Emergency myelopoiesis arises to cope with an increased demand from the organism to replenish myeloid cells at the site of infection (17). Our study supports the concept that emergency myelopoiesis may also constitute a demand-adapted response to deal with excessive inflammation and immunopathology (23, 55). Our observation is reminiscent with a population of monocytes that have been shown to be remotely educated by IFN- γ within the BM for regulatory functions upon *Toxoplasma gondii*-induced gut infection (55). Therefore, sensing of IFN- γ by differentiating myeloid cells from multiple lineages could represent a broader regulatory mechanism during infections at mucosal surfaces. While IFN- γ is a

prototypical inflammatory cytokine, it may also be part of a feedback circuit to limit immunopathology. The molecular and cellular actors that regulate this IAV-dependent IFN- γ response in the BM have not been explored. BM-resident innate (T) lymphocytes are interesting candidates as they were shown to produce IFN- γ upon innate signals (55, 56). It also remains unclear why only a fraction of BM neutrophils acquires a regulatory profile during experimental VRI. Although this may suggest the existence of a precommitted precursor, one can argue that the levels of IFN- γ are limiting in the BM during IAV infection. In line, the use of IFN- γ enabled to generate BMN with uniform regulatory phenotype.

The presence of a substantial proportion of PD-L1⁺ neutrophils in several nonlymphoid tissues [e.g., lungs, liver, and gut (fig.S9)]—but

not in spleen or lymph nodes (fig. S9)—under steady-state condition may suggest homeostatic functions in tissues exposed to numerous antigens, in which a high level of regulation and/or tolerance is required.

However, upon IAV infection, no increase in PD-L1⁺ neutrophils could be noted in nonlymphoid tissues, at the exception of the lungs, suggesting their preferential migration toward inflamed tissues. In line, BM PD-L1⁺ neutrophils from IAV-infected mice readily expressed the integrin CD49d (28). Thus, BM PD-L1⁺ neutrophils appear to be equipped to migrate to inflamed tissue upon inflammation/infection, and therefore, this may explain why the relatively low proportion of PD-L1⁺ neutrophils in the BM (~10% of total neutrophils) can give rise to a large proportion of PD-L1⁺ neutrophils in the lungs of infected mice. We cannot rule out the contribution of other factors such as a high capacity to proliferate and/or the acquisition of the PD-L1⁺ phenotype once in the lungs. This latest hypothesis is nevertheless unlikely since lung PD-L1⁻ and PD-L1⁺ neutrophils presented highly divergent transcriptomes suggesting discrete sublineages. However, it is possible that additional signals received in the lungs can further tune PD-L1⁺ neutrophil functions. Our data suggest that the regulatory properties of PD-L1⁺ neutrophils varied during the course of IAV infection. For instance, the production of Arg-1 by lung PD-L1⁺ neutrophils is rather limited during the inflammatory phase and prevails during the resolution phase. This suggests that additional layers of regulation influence the functions of PD-L1⁺ neutrophils.

Moreover, their presence in naive mice in the absence of strong IFN- γ signaling suggests the involvement of other factor(s) in the acquisition of the regulatory program. For instance, generation of BMN favors the PD-L1⁺ profile even in the absence of IFN- γ , pointing toward other factor(s). Others factors such as granulocyte colony-stimulating factor (G-CSF) and transforming growth factor- β (TGF- β) have been involved in the generation of PD-L1⁺ neutrophils with regulatory/suppressive functions upon thermal injury (16) or cancer (57, 58). TGF- β -dependent expansion of PD-L1⁺ neutrophils occurs in the periphery and is transient (irrespective of cell death) (16). Thus, it is likely that the biology of the regulatory/suppressive neutrophils may greatly vary according to the signals involved and tissue location. Further works into the licensing mechanisms leading to regulatory functions in neutrophils will undoubtedly offer new insights into how signals can be temporally and spatially coordinated and integrated to control the inflammatory balance. This is of particular interest during severe viral pneumonia/ARDS in which the therapeutic window has to be carefully considered for immunomodulatory approaches.

MATERIALS AND METHODS

Clinical study design, patient population, and approval

Over 18-year-old patients with severe pneumonia and admitted in intensive care unit were prospectively included in this study, from January 2018 to May 2020. Sample collection was performed within 48 hours upon admission in intensive care unit. Only patients with viral infection without concomitant diagnosed bacterial infections were studied in the present work. The clinical characteristics of the patients are documented in Table 1. The study was conducted in the University hospital of Tours (France). All patients or their next of kin gave their consent for enrollment in the study (ClinicalTrials.gov identifier: NCT03379207). This study was approved by the national

ethic committee “Comité de Protection des Personnes Ile-de-France 8” under the agreement number 2017-A01841-52, in accordance with the French laws. Blood samples from healthy donors were obtained from the “Etablissement Français du Sang” (agreement: CPDL-PLER-2019 188).

Mice

Inbred and sex-matched 8- to 10-week-old C57BL/6j mice were purchased from Janvier (Le Genest-St-Isle, France) and maintained at the University of Tours under specific pathogen-free conditions. *Ifng*^{-/-} and control mice were maintained at the Pasteur Institute of Lille under specific pathogen-free conditions. *Ifngr1*^{-/-} mice were provided by F. Laurent (INRAE, Nouzilly, France). All animal work was conformed to the French governmental and committee guidelines for the care and use of animals for scientific purposes and was approved by the national ethic committee under approval number 201611151159949.

Reagents and antibodies

The following are mAbs against mouse CD11b (M1/70), CD45 (30-f11), CD49d (R1-2), Sca-1 (D7), PD-L1/CD274 (10F.9G2), Arginase-1 (A1exF5), MHC-II (NIMR-4), Ly6G (1A8), CXCR4/CD184 (L276F12), F4/80 (BM8), IFN- γ R1/CD119 (2E2), CD64 (X54-5/7.1), Ly6C (HK1.4), and Siglec F (E50-2440). The following are mAbs against human CD16 (3G8), CD14 (M5E2), PD-L1/CD274 (29E.2A3), and CD10 (HI10a). All mAbs and appropriated isotype controls were purchased from BioLegend (Amsterdam, The Netherlands), BD Pharmingen (Le Pont de Claix, France), and Thermo Fisher Scientific/eBioscience (Paris, France). Dead cells were excluded with a LIVE/DEAD Fixable Aqua Dead Cell Stain kit (Thermo Fisher Scientific, Illkirch, France). Mouse enzyme-linked immunosorbent assay kits were from R&D Systems (Lille, France) and eBioscience. The Lineage Cell Depletion Kit was from Miltenyi Biotec (Paris, France). Stem cell factor (SCF), IL-3, and G-CSF were purchased from Miltenyi Biotec. Purified anti-mouse CD3 (145-2C11) was from BD Pharmingen. Anti-mouse PD-L1 (clone 10F.9G2), anti-mouse Ly6G (1A8), and isotype controls were from Bio X Cell (Lebanon, NH, USA). A Cell Trace Violet (CTV) cell proliferation kit was from Thermo Fisher Scientific. Reparixin was from Sigma-Aldrich (Saint-Quentin-Fallavier, France). rmIFN- γ was purchased from Thermo Fisher Scientific.

IAV infection

The H3N2 IAV strain (A/Scotland/20/74) has been described elsewhere (59). Mice were anesthetized and administered intranasally with 40 μ l of phosphate-buffered saline (PBS) containing 150 plate-forming units. Weight and survival were monitored every second day following infection.

Tissue harvest and preparation of cell suspensions

Lung cells were prepared as previously described (60). Briefly, lungs were perfused with saline injected into the right ventricle. Lungs were harvested and minced using a gentleMACS dissociator (Miltenyi Biotec) in a medium containing Liberase (125 μ g/ml; Roche; Meylan, France) and deoxyribonuclease type I (100 μ g/ml; Roche). Lung homogenates were next resuspended in PBS and filtered onto a 100- μ m cell strainer (Dutscher). Pellets were recovered in PBS 2% fetal calf serum (FCS), and erythrocytes were removed using a red blood cell lysis buffer (Sigma-Aldrich) before being filtered onto a

40- μm cell strainer (Dutscher). Bronchoalveolar lavages (BAL) were performed after tracheal catheterization by injecting four times 0.5 ml of cold PBS. BAL were then centrifuged at 400g for 5 min, and pellets were recovered in PBS 2% FCS. Erythrocytes were removed using a red blood cell lysis buffer (Sigma-Aldrich) before being filtered onto a 40- μm cell strainer. For analysis of BM cells, femurs and tibias were collected and cut at their extremities, and cold RPMI was injected to harvest BM core biopsy, which was mechanically disrupted onto a 100- μm cell strainer. After centrifugation (400g for 5 min), erythrocytes were removed before being filtered onto a 40- μm cell strainer. For mRNA expression experiments, BM core biopsy was immediately frozen in liquid nitrogen. Blood was collected in microtubes filled with 30 μl of heparin from the retro-orbital sinus, while mice were anesthetized. Erythrocytes were removed upon several washes in a red blood cell lysis buffer (Sigma-Aldrich).

For human neutrophil analyses, total blood was subjected to three repeated steps of erythrocyte lysis. ETA were collected from intubated patients and incubated with dithiothreitol (1 mM) in PBS (5 ml/g of ETA) for 30 min under continuous agitation. After centrifugation, pellet cells were filtered onto a 100- μm cell strainer. After removing red blood cells, cells were passed through a 40- μm cell strainer prior analysis.

Oxidant production assay

Oxidant reactive nitrogen species/reactive oxygen species (RNS/ROS) production by neutrophils was assessed by flow cytometry using dihydro-rhodamine123 (DHR123). Lung homogenates were incubated with or without 100 nM phorbol 12-myristate 13-acetate (PMA) and with 1 μM DHR123 for 5 min at 37°C before analysis.

In vitro neutrophil differentiation

Progenitors from the BM were enriched using the Lineage Cell Depletion Kit (Miltenyi Biotec). The negative fraction was then seeded into a six-well plate at 1×10^5 cell/ml in complete Iscove's Modified Dulbecco's Medium (IMDM) medium. Cells were differentiated for 7 days in the presence of SCF (50 ng/ml), IL-3 (50 ng/ml), and G-CSF (50 ng/ml) as previously described (61). In some cases, mouse recombinant IFN- γ (1 ng/ml) was added into the culture on days 0, 3, and 5.

Proliferation assay

C57BL/6j mice were intranasally infected with IAV [150 plaque-forming units (PFU)], and lungs were collected at 8 dpi. Neutrophils were then enriched using an anti-Ly6G MicroBead kit (Miltenyi Biotec). In parallel, CTV-labeled spleen cells (5×10^5) from naive mice were stimulated with plate-bound anti-CD3 mAb (4 $\mu\text{g}/\text{ml}$, clone 145-2C11) in a 96-well culture plate in complete 10% FCS RPMI 1640 medium. Enriched neutrophils were then cocultured with anti-CD3-stimulated spleen cells for 48 hours in the presence of immunoglobulin (Ig) control (10 $\mu\text{g}/\text{ml}$, clone LTF-2) or anti-PD-L1 (10 $\mu\text{g}/\text{ml}$, clone 10F9G2) mAbs. Cells were then stained with anti-CD45, anti-CD3, anti-CD4, anti-CD8 antibodies, and T cell proliferation rate was measured by monitoring loss of CTV fluorescence intensity.

Flow cytometry

Cells were stained with appropriate dilutions of mAbs. Then, cells were washed and, in some cases, fixed and permeabilized using a commercial kit from eBioscience according to the manufacturer's

information. Dead cells were excluded using the LIVE/DEAD Cell Staining kit. Cells were acquired on either a LSR Fortessa cytometer (BD Biosciences) or a MACS Quant (Miltenyi Biotec). Analyses were performed using the VenturiOne software (Applied Cytometry, Sheffield, UK).

Cell sorting and in vitro/ex vivo assays

To purify neutrophil subsets, lung mononuclear cells were labeled with fluorescein isothiocyanate-conjugated anti-Ly6G mAb, PerCp-Cy5.5-conjugated anti-CD11b mAb, and allophycocyanin (APC)-conjugated anti-PD-L1 mAb. After cell surface labeling, cells were sorted using a FACSMelody (BD Biosciences). This protocol yielded >98% cell purity. For in vitro stimulation assays, 5×10^4 neutrophil subsets were cultured for 4 hours in complete RPMI 5% FCS in the absence of any additional stimulation. In some cases, neutrophils were pulsed for 5 min with PMA. Then, supernatants were harvested for further analyses, and/or cells were subjected to cytometry analysis.

Single-cell RNA sequencing and data preprocessing

Single-cell suspension from five lungs of IAV-infected mice (day 11) was pooled, and neutrophil subsets (LiveDead⁻ CD45⁺ SiglecF⁻ CD11b⁺ Ly6G⁺ PD-L1^{+/-}) were sorted on a FACSMelody (BD Biosciences) (purity > 99%) into 1 \times PBS with 0.04% bovine serum albumin + ribonuclease inhibitor. Sorted cells were counted under a microscope, and 8000 to 10,000 cells per subset were loaded onto a Chromium controller (10X Genomics). Reverse transcription and library preparation were performed according to the manufacturer's protocol. Libraries were simultaneously sequenced on a NovaSeq 6000. Cell Ranger Single-Cell Software Suite v2.0.0 was used to perform sample demultiplexing, barcode processing, and single-cell 30 gene counting using standard default parameters and *Mus musculus* build mm10. The argument “-force-cell” was used according to 10X Genomics recommendations (<https://support.10xgenomics.com/single-cell-gene-expression/software/pipelines/latest/tutorials/neutrophils>).

Single-cell RNA sequencing analysis

Cell and gene filtering

Raw gene expression matrices generated per sample were passed to Seurat for preprocessing. Cells with less than 90 unique molecular identifiers(UMI) and more than 5% of mitochondrial RNA were removed; then, transcripts expressed in less than three cells were removed. Cells considered as doublet were also removed using DoubletFinder (62). Thus, we could retain 1165 cells from the PDL-1⁻ subset and 1834 cells from the PD-L1⁺ subset. Concordance between datasets enabled to merge them for downstream analyses. Standard processing was used with an UMAP with $k = 50$ and $\text{min.dist} = 0.3$ using 20 principle components.

Trajectory analysis

Seurat dataset was converted into SingleCellExperiment to run trajectory analysis. All data from Monocle3 object were passed to Seurat.

Mapping gene along pseudotime

Pseudotime was calculated using Monocle3, and pseudotime values were passed to Seurat object. Cells were ordered by pseudotime values. Spearman correlation was calculated for all genes with pseudotime. Top 20 highly positively and negatively correlated genes have been chosen to characterize the maturation of neutrophils.

Plots

All feature plots were created using scCustomize package. Density plots were made using Nebulosa package with “wkde” as kernel density estimation method (63). ClusterMap was made using scanpy (64). GO enrichment analysis was performed using ClusterProfiler2. The following GO datasets have been used: regulation of gene expression (GO: 0010468), regulation of cytoskeleton organization (GO: 0051493), cell cycle process (GO: 0022402), negative regulation of execution phase of apoptosis (GO: 1900118), neutrophil-mediated antimicrobial response (GO: 0070944), positive regulation of the inflammatory response (GO: 0050729), negative regulation of the inflammatory response (GO: 0050728), and IFN- γ -mediated signaling pathway (GO: 0060333). All gene sets can be found at <https://gsea-msigdb.org/gsea/msigdb/mouse/genesets.jsp?collection=GO>.

Analysis of gene transcripts by quantitative reverse transcription polymerase chain reaction

RNAs from whole lungs or BM of naive or IAV-infected mice were extracted and purified using the NucleoSpin RNA Extraction Kit (Macherey-Nagel) according to the manufacturer’s instructions. cDNAs were synthesized using a High Capacity RNA-to-cDNA kit (Thermo Fisher Scientific), and quantitative reverse transcription polymerase chain reaction (PCR) was carried out using specific primers (table S2) and SYBR Green PCR Master Mix (QIAGEN). PCR amplification of *Gapdh* was performed to control for sample loading and normalization between samples. Δ Ct values were obtained by deducting Ct values of *Gapdh* mRNA from the Ct values obtained for the investigated genes. Data are represented as relative expression of mRNA levels.

Neutrophil depletion and PD-L1 blockade

Neutrophils were depleted using 1A8 (150 μ g per mouse i.p. in 200 μ l of PBS) every second day from 4 dpi. The 10F.9G2 was injected (200 μ g per mouse i.p. in 200 μ l of PBS) every second day from 4 dpi. A rat IgG2a (1A3) and a rat IgG2b (LTF2) isotype control antibodies were used as controls.

Assessment of the pathology

For histological examination, total lungs were fixed by gentle inflation and immersion in PBS containing 3.2% paraformaldehyde and embedded in paraffin. Fixed lung slices (5 μ m) were subjected to H&E staining. A blinded examiner evaluated extent of immunopathology based on leukocyte recruitment, the presence of hyaline membranes, thickness of alveolar septa, and filling the airspace with proteinaceous debris.

Statistical analysis

All statistical analysis was performed using GraphPad Prism software. The statistical significance was evaluated using nonparametric Mann-Whitney *U* tests or Kruskal-Wallis to compare the means of biological replicates in each experimental group. Survival rates were analyzed using a log-rank test. Results with a *P* value of less than 0.05 were considered significant. ns indicates not significant; **P* < 0.05, ***P* < 0.01, and ****P* < 0.001.

Supplementary Materials

The PDF file includes:

Figs. S1 to S9

Legend for table S1

Table S2

Other Supplementary Material for this manuscript includes the following:

Table S1

REFERENCES AND NOTES

1. A. H. Newton, A. Cardani, T. J. Braciale, The host immune response in respiratory virus infection: Balancing virus clearance and immunopathology. *Semin. Immunopathol.* **38**, 471–482 (2016).
2. B. T. Thompson, R. C. Chambers, K. D. Liu, Acute respiratory distress syndrome. *N. Engl. J. Med.* **377**, 562–572 (2017).
3. M. A. Matthay, R. L. Zemans, G. A. Zimmerman, Y. M. Arabi, J. R. Beitler, A. Mercat, M. Herridge, A. G. Randolph, C. S. Calfee, Acute respiratory distress syndrome. *Nat. Rev. Dis. Primers.* **5**, 18 (2019).
4. S. K. Ahuja, M. S. Manoharan, G. C. Lee, L. R. McKinnon, J. A. Meunier, M. Steri, N. Harper, E. Fiorillo, A. M. Smith, M. I. Restrepo, A. P. Branum, M. J. Bottomley, V. Orru, F. Jimenez, A. Carrillo, L. Pandrangi, C. A. Winter, L. A. Winter, A. A. Gaitan, A. G. Moreira, E. A. Walter, G. Silvestri, C. L. King, Y.-T. Zheng, H.-Y. Zheng, J. Kimani, T. Blake Ball, F. A. Plummer, K. R. Fowke, P. N. Harden, K. J. Wood, M. T. Ferris, J. M. Lund, M. T. Heise, N. Garrett, K. R. Canady, S. S. Abdool Karim, S. J. Little, S. Gianella, D. M. Smith, S. Letendre, K. D. Richman, F. Cucca, H. Trinh, S. Sanchez-Reilly, J. M. Hecht, J. A. Cadena Zuluaga, A. Anzueto, J. A. Pugh, South Texas Veterans Health Care System COVID-19 team, M. I. Abdalla, S. G. Adams, Y. Adebayo, J. Agnew, S. Ali, G. Anstead, M. Balmes, J. Barker, D. Baruch-Bienen, V. Bible, A. Birdwell, S. Braddy, S. Bradford, H. Briggs, J. M. Corral, J. J. Dacus, P. J. Danaher, S. A. DePaul, J. Dickerson, J. Doanne, A. Ehsan, S. Elbel, M. Escalante, C. Escamilla, V. Escamilla, R. Farrar, D. Feldman, D. Flores, J. Flynn, D. Ford, J. D. Foy, M. Freeman, S. Galley, J. Garcia, M. Garza, S. Gilman, M. Goel, J. Gomez, V. K. Goyal, S. Grassmuck, S. Grigsby, J. Hanson, B. Harris, A. Haywood, C. Hinojosa, T. T. Ho, T. Hopkins, L. L. Horvath, A. N. Hussain, A. Jabur, P. Jewell, T. B. Johnson, A. C. Lawler, M. Lee, C. S. Lester, S. M. Levine, H. V. Lewis, A. Louder, C. Mainor, R. Maldonado, C. Martinez, Y. Martinez, D. Maselli, C. Mata, N. McElligott, L. Medlin, M. Mireles, J. Moreno, K. Morneau, J. Muetz, S. B. Munro, C. Murray, A. Nambiar, D. Nassery, R. Nathanson, K. Oakman, J. O’Rourke, C. Padgett, S. Pascual-Guardia, M. Patterson, G. L. Perez, R. Perez, R. Perez III, R. E. Phillips, P. B. Polk, M. A. Pomager, K. J. Preston, K. C. Proud, M. Rangel, T. A. Ratcliffe, R. L. Reichelderfer, E. M. Renz, J. Ross, T. Rudd, M. E. Sanchez, T. Sanders, K. C. Schindler, D. Schmit, R. T. Sehgal, C. Solorzano, N. Soni, W. S. Tam, E. J. Tovar, S. A. Trammell Velasquez, A. R. Tyler, A. Vasquez, M. C. Veloso, S. G. Venticinque, J. A. Villalpando, M. Villanueva, L. Villegas, M. Walker, A. Wallace, M. Wallace, E. Wang, S. Wickizer, A. Williamson, A. Yunes, K. H. Zentner, B. K. Agan, R. Root-Bernstein, R. A. Clark, J. F. Okulicz, W. He, Immune resilience despite inflammatory stress promotes longevity and favorable health outcomes including resistance to infection. *Nat Commun* **14**, 3286 (2023).
5. T. Flerlage, D. F. Boyd, V. Meliopoulos, P. G. Thomas, S. Schultz-Cherry, Influenza virus and SARS-CoV-2: Pathogenesis and host responses in the respiratory tract. *Nat. Rev. Microbiol.* **19**, 425–441 (2021).
6. A. E. Williams, R. C. Chambers, The mercurial nature of neutrophils: Still an enigma in ARDS? *Am. J. Physiol. Lung Cell. Mol. Physiol.* **306**, L217–L230 (2014).
7. J. Schulte-Schrepping, N. Reusch, D. Paclik, K. Baßler, S. Schlickeiser, B. Zhang, B. Krämer, T. Krammer, S. Brumhard, L. Bonaguro, E. de Domenico, D. Wendisch, M. Grasshoff, T. S. Kapellos, M. Beckett, T. Pecht, A. Saglam, O. Dietrich, H. E. Mei, A. R. Schulz, C. Conrad, D. Kunkel, E. Vafadarnejad, C.-J. Xu, A. Horne, M. Herbert, A. Drews, C. Thibeault, M. Pfeiffer, S. Hippenstiel, A. Hocke, H. Müller-Redetzky, K.-M. Heim, F. Machleidt, A. Uhrig, L. Bosquillon de Jarcy, L. Jürgens, M. Stegemann, C. R. Glösenkamp, H.-D. Volk, G. Goffinet, M. Landthaler, E. Wylar, P. Georg, M. Schneider, C. Dang-Heine, N. Neuwinger, K. Kappert, R. Tauber, V. Corman, J. Raabe, K. M. Kaiser, M. T. Vinh, G. Rieke, C. Meisel, T. Ulas, M. Becker, R. Geffers, M. Witzernath, C. Drosten, N. Suttrop, C. von Kalle, F. Kurth, K. Händler, J. L. Schultze, A. C. Aschenbrenner, Y. Li, J. Nattermann, B. Sawitzki, A.-E. Saliba, L. E. Sander, A. Angelov, R. Bals, A. Bartholomäus, A. Becker, D. Bezdán, E. Bonifacio, P. Bork, T. Clavel, M. Colome-Tatche, A. Diefenbach, A. Diltney, N. Fischer, K. Förstner, J. S. Frick, J. Gagneur, A. Goemann, T. Hain, M. Hummel, S. Janssen, J. Kalinowski, R. Kallies, B. Kehr, A. Keller, S. Kim-Hellmuth, C. Klein, O. Kohlbacher, J. O. Korbel, I. Kurth, M. Landthaler, Y. Li, K. Ludwig, O. Makarewicz, M. Marz, A. McHardy, C. Mertes, M. Nöthen, P. Nürnberg, U. Ohler, S. Ossowski, J. Overmann, S. Peter, K. Pfeiffer, A. R. Poetsch, A. Pühler, N. Rajewsky, M. Ralsor, O. Rieß, S. Ripke, U. Nunes da Rocha, P. Rosenstiel, A. E. Saliba, L. E. Sander, B. Sawitzki, P. Schiffer, E. C. Schulte, J. L. Schultze, A. Szczyba, O. Stegle, J. Stoye, F. Theis, J. Vehreschild, J. Vogel, M. von Kleist, A. Walker, J. Walter, D. Wiczorek, J. Ziebuhr, Deutsche COVID-19 OMICS Initiative (DeCOI), severe COVID-19 is marked by a dysregulated myeloid cell compartment. *Cell* **182**, 1419–1440. e23 (2020).
8. A. Silvin, N. Chapuis, G. Dunsmore, A.-G. Goubet, A. Dubuisson, L. Derosa, C. Almire, C. Hénon, O. Kosmider, N. Droin, P. Rameau, C. Catelain, A. Alfaro, C. Dussiau, C. Friedrich, E. Sourdeau, N. Marin, T.-A. Szwebel, D. Cantin, L. Mouthon, D. Borderie, M. Deloger, D. Bredel, S. Mouraud, D. Drubay, M. Andrieu, A.-S. Lhonneur, V. Saada, A. Stoclin, C. Willekens, F. Pommeret, F. Griscelli, L. G. Ng, Z. Zhang, P. Bost, I. Amit, F. Barlesi, A. Marabelle, F. Pène, B. Gachot, F. André, L. Zitvogel, F. Ginhoux, M. Fontenay, E. Solary,

- Elevated calprotectin and abnormal myeloid cell subsets discriminate severe from mild COVID-19. *Cell* **182**, 1401–1418.e18 (2020).
9. F. P. Veras, M. C. Pontelli, C. M. Silva, J. E. Toller-Kawahisa, M. de Lima, D. C. Nascimento, A. H. Schneider, D. Caetité, L. A. Tavares, I. M. Paiva, R. Rosales, D. Colón, R. Martins, I. A. Castro, G. M. Almeida, M. I. F. Lopes, M. N. Benatti, L. P. Bonjorno, M. C. Giannini, R. Luppino-Assad, S. L. Almeida, F. Vilar, R. Santana, V. R. Bollela, M. Auxiliadora-Martins, M. Borges, C. H. Miranda, A. Pazin-Filho, L. L. P. da Silva, L. D. Cunha, D. S. Zamboni, F. Dal-Pizzolo, L. O. Leiria, L. Siyuan, S. Batah, A. Fabro, T. Mauad, M. Dolnikoff, A. Duarte-Neto, P. Saldiva, T. M. Cunha, J. C. Alves-Filho, E. Arruda, P. Louzada-Junior, R. D. Oliveira, F. Q. Cunha, SARS-CoV-2-triggered neutrophil extracellular traps mediate COVID-19 pathology. *J Exp Med* **217**, e20201129 (2020).
 10. M. Brandes, F. Klauschen, S. Kuchen, R. N. Germain, R. N. G. Marlène Brandes, F. Klauschen, S. Kuchen, M. Brandes, F. Klauschen, S. Kuchen, R. N. Germain, R. N. G. M. Brandes, F. Klauschen, S. Kuchen, M. Brandes, F. Klauschen, S. Kuchen, R. N. Germain, A systems analysis identifies a feedforward inflammatory circuit leading to lethal influenza infection. *Cell* **154**, 197–212 (2013).
 11. B. G. Yipp, P. Kubes, NETosis: How vital is it? *Blood* **122**, 2784–2794 (2013).
 12. P. S. Pillai, R. D. Molony, K. Martinod, H. Dong, I. K. Pang, M. C. Tal, A. G. Solis, P. Bielecki, S. M. Borge, M. Trentalange, R. A. Homer, R. A. Flavell, D. D. Wagner, R. R. Montgomery, A. C. Shaw, P. Staeheli, A. Iwasaki, Mx1 reveals innate pathways to antiviral resistance and lethal influenza disease. *Science* **352**, 463–466 (2016).
 13. T. Narasaraaju, E. Yang, R. P. Samy, H. H. Ng, W. P. Poh, A.-A. Liew, M. C. Phoon, N. van Rooijen, V. T. Chow, Excessive neutrophils and neutrophil extracellular traps contribute to acute lung injury of influenza pneumonitis. *Am. J. Pathol.* **179**, 199–210 (2011).
 14. I. Puga, M. Cols, C. M. Barra, B. He, L. Cassis, M. Gentile, L. Comerma, A. Chorny, M. Shan, W. Xu, G. Magri, D. M. Knowles, W. Tam, A. Chiu, J. B. Bussel, S. Serrano, J. A. Lorente, B. Bellosillo, J. Lloreta, N. Juanpere, F. Alameda, T. Baró, C. D. de Heredia, N. Torán, A. Català, M. Torredadell, C. Fortuny, V. Cusi, C. Carreras, G. A. Diaz, J. M. Blander, C.-M. Farber, G. Silvestri, C. Cunningham-Rundles, M. Calvillo, C. Dufour, L. D. Notarangelo, V. Lougaris, A. Plebani, J.-L. Casanova, S. C. Ganai, A. Diefenbach, J. I. Aróstegui, M. Juan, J. Yagüe, N. Mahlaoui, J. Donadieu, K. Chen, A. Cerutti, B cell-helper neutrophils stimulate the diversification and production of immunoglobulin in the marginal zone of the spleen. *Nat Immunol* **13**, 170–180 (2011).
 15. B. McDonald, K. Pittman, G. B. Menezes, S. A. Hirota, I. Slaba, C. C. M. Waterhouse, P. L. Beck, D. A. Muruve, P. Kubes, Intravascular danger signals guide neutrophils to sites of sterile inflammation. *Science* **330**, 362–366 (2010).
 16. A. Thanabalasuriar, A. J. Chiang, C. Morehouse, M. Camara, S. Hawkins, A. E. Keller, A. C. Kiskal, C. S. Caceres, A. A. Berlin, N. Holowecy, V. N. Takahashi, L. Cheng, M. de Los Reyes, M. Pelletier, A. C. Patera, B. Sellman, S. Hess, M. Marelli, C. C. Boo, T. S. Cohen, A. DiGiandomenico, PD-L1⁺ neutrophils contribute to injury-induced infection susceptibility. *Sci Adv* **7**, eabd9436 (2021).
 17. M. G. Manz, S. Boettcher, Emergency granulopoiesis. *Nat. Rev. Immunol.* **14**, 302–314 (2014).
 18. O. Marini, S. Costa, D. Bevilacqua, F. Calzetti, N. Tamassia, C. Spina, D. De Sabata, E. Tinazzi, C. Lunardi, M. T. Scupoli, C. Cavallini, E. Zoratti, I. Tinazzi, A. Marchetta, A. Vassanelli, M. Cantini, G. Gandini, A. Ruzzenente, A. Guglielmi, F. Missale, W. Vermi, C. Tecchio, M. A. Cassatella, P. Scapini, Mature CD10⁺ and immature CD10⁻ neutrophils present in G-CSF-treated donors display opposite effects on T cells. *Blood* **129**, 1343–1356 (2017).
 19. R. Le Goffic, V. Balloy, M. Lagranderie, L. Alexopoulou, N. Escriou, R. Flavell, M. Chignard, M. Si-Tahar, Detrimental contribution of the Toll-like receptor (TLR)3 to influenza A virus-induced acute pneumonia. *PLOS Pathog.* **2**, e53 (2006).
 20. R. Grieshaber-Bouyer, F. A. Radtke, P. Cunin, G. Stifano, A. Levescot, B. Vijaykumar, N. Nelson-Maney, R. B. Blaustein, P. A. Monach, P. A. Nigrovic, ImmGen Consortium, O. Aguilar, R. Allan, J. Astarita, K. F. Austen, N. Barrett, A. Baysoy, C. Benoist, B. D. Brown, M. Buechler, J. Buenrostro, M. A. Casanova, K. Chowdhary, M. Colonna, T. Crowl, T. Deng, F. Desland, M. Dhainaut, J. Ding, C. Dominguez, D. Dwyer, M. Frascoli, S. Gal-Oz, A. Goldrath, T. Johanson, S. Jordan, J. Kang, V. Kapoor, E. Kenigsberg, J. Kim, K. Kim, E. Kiner, M. Kronenberg, L. Lanier, C. Laplace, C. Lareau, A. Leader, J. Lee, A. Magen, B. Maier, A. Maslova, D. Mathis, A. McFarland, M. Merad, E. Meunier, P. A. Monach, S. Mostafavi, S. Muller, C. Muus, H. Ner-Gaon, Q. Nguyen, G. Novakovsky, S. Nutt, K. Omilusik, A. Ortiz-Lopez, M. Paynich, V. Peng, M. Potempa, R. Pradhan, S. Quon, R. Ramirez, D. Ramanan, G. Randolph, A. Regev, S. A. Rose, K. Seddu, T. Shay, A. Shemesh, J. Shyer, C. Smilie, N. Spidale, A. Subramanian, K. Sylvia, J. Tellier, S. Turley, B. Vijaykumar, A. Wagers, C. Wang, P. L. Wang, A. Wroblewska, L. Yang, A. Yim, H. Yoshida, The neutrotome transcriptional signature defines a single continuum of neutrophils across biological compartments. *Nat. Commun.* **12**, 2856 (2021).
 21. V. Y. Kiselev, K. Kirschner, M. T. Schaub, T. Andrews, A. Yiu, T. Chandra, K. N. Natarajan, W. Reik, M. Barahona, A. R. Green, M. Hemberg, SC3: Consensus clustering of single-cell RNA-seq data. *Nat. Methods* **14**, 483–486 (2017).
 22. A. J. Ozga, M. T. Chow, A. D. Luster, Chemokines and the immune response to cancer. *Immunity* **54**, 859–874 (2021).
 23. M. Evrard, I. W. H. Kwok, S. Z. Chong, K. W. W. Teng, E. Becht, J. Chen, J. L. Sieow, H. L. Penny, G. C. Ching, S. Devi, J. M. Adrover, J. L. Y. Li, K. H. Liang, L. Tan, Z. Poon, S. Foo, J. W. Chua, I.-H. Su, K. Balabanian, F. Bacheleerie, S. K. Biswas, A. Larbi, W. Y. K. Hwang, V. Madan, H. P. Koeffler, S. C. Wong, E. W. Newell, A. Hidalgo, F. Ginhoux, L. G. Ng, Developmental analysis of bone marrow neutrophils reveals populations specialized in expansion, trafficking, and effector functions. *Immunity* **48**, 364–379.e8 (2018).
 24. S. Jaillon, A. Ponzetta, D. Di Mitri, A. Santoni, R. Bonecchi, A. Mantovani, Neutrophil diversity and plasticity in tumour progression and therapy. *Nat. Rev. Cancer* **20**, 485–503 (2020).
 25. C. Trapnell, D. Cacchiarelli, J. Grimsby, P. Pokharel, S. Li, M. Morse, N. J. Lennon, K. J. Livak, T. S. Mikkelsen, J. L. Rinn, The dynamics and regulators of cell fate decisions are revealed by pseudotemporal ordering of single cells. *Nat. Biotechnol.* **32**, 381–386 (2014).
 26. S. Jaiswal, C. H. M. Jamieson, W. W. Pang, C. Y. Park, M. P. Chao, R. Majeti, D. Traver, N. van Rooijen, I. L. Weissman, CD47 is upregulated on circulating hematopoietic stem cells and leukemia cells to avoid phagocytosis. *Cell* **138**, 271–285 (2009).
 27. V. Bronte, P. Serafini, A. Mazzoni, D. M. Segal, P. Zanovello, L-arginine metabolism in myeloid cells controls T-lymphocyte functions. *Trends Immunol.* **24**, 302–306 (2003).
 28. S. Paudel, P. Baral, L. Ghimire, S. Bergeron, L. Jin, J. A. DeCorte, J. T. Le, S. Cai, S. Jeyaseelan, CXCL1 regulates neutrophil homeostasis in pneumonia-derived sepsis caused by *Streptococcus pneumoniae* serotype 3. *Blood* **133**, 1335–1345 (2019).
 29. Y. Liu, D. Merlin, S. L. Burst, M. Pochet, J. L. Madara, C. A. Parkos, The role of CD47 in neutrophil transmigration. Increased rate of migration correlates with increased cell surface expression of CD47. *J Biol Chem* **276**, 40156–40166 (2001).
 30. K. J. Eash, A. M. Greenbaum, P. K. Gopalan, D. C. Link, CXCR2 and CXCR4 antagonistically regulate neutrophil trafficking from murine bone marrow. *J. Clin. Invest.* **120**, 2423–2431 (2010).
 31. S. von Vietinghoff, M. Asagiri, D. Azar, A. Hoffmann, K. Ley, Defective regulation of CXCR2 facilitates neutrophil release from bone marrow causing spontaneous inflammation in severely NF- κ B-deficient mice. *J. Immunol.* **185**, 670–678 (2010).
 32. J. H. DeLong, A. O. Hall, C. Konradt, G. M. Coppock, J. Park, G. Harms Pritchard, C. A. Hunter, Cytokine- and TCR-mediated regulation of T cell expression of Ly6C and Sca-1. *J. Immunol.* **200**, 1761–1770 (2018).
 33. T. J. Moraes, J. H. Zurawska, G. P. Downey, Neutrophil granule contents in the pathogenesis of lung injury. *Curr. Opin. Hematol.* **13**, 21–27 (2006).
 34. T. Schmitz, K. Guo, J. K. Tripathi, Z. Wang, B. McGregor, M. Klomp, G. Ambigapathy, R. Mathur, J. Hur, M. Pichichero, J. Kolls, M. N. Khan, Interferon- γ promotes monocyte-mediated lung injury during influenza infection. *Cell Rep.* **38**, 110456 (2022).
 35. B. M. Coates, K. L. Staricha, C. M. Koch, Y. Cheng, D. K. Shumaker, G. R. S. Budinger, H. Perlman, A. V. Misharin, K. M. Ridge, Alveolar macrophages drive influenza A virus-mediated lung injury in juvenile mice. *J. Immunol.* **200**, 2391–2404 (2018).
 36. S.-J. Lin, M. Lo, R.-L. Kuo, S.-R. Shih, D. M. Ojcius, J. Lu, C.-K. Lee, H.-C. Chen, M. Y. Lin, C.-M. Leu, C.-N. Lin, C.-H. Tsai, The pathological effects of CCR2+ inflammatory monocytes are amplified by an IFNAR1-triggered chemokine feedback loop in highly pathogenic influenza infection. *J. Biomed. Sci.* **21**, 99 (2014).
 37. S. Duan, P. G. Thomas, Balancing immune protection and immune pathology by CD8(+) T-cell responses to influenza infection. *Front. Immunol.* **7**, 25 (2016).
 38. G. Zhou, S. W. Juang, K. P. Kane, NK cells exacerbate the pathology of influenza virus infection in mice. *Eur. J. Immunol.* **43**, 929–938 (2013).
 39. F.-F. Huang, P. F. Barnes, Y. Feng, R. Donis, Z. C. Chronoes, S. Idell, T. Allen, D. R. Perez, J. A. Whitsett, K. Dunussi-Joannopoulos, H. Shams, GM-CSF in the lung protects against lethal influenza infection. *Am. J. Respir. Crit. Care Med.* **184**, 259–268 (2011).
 40. A. Cardani, A. Boulton, T. S. Kim, T. J. Braciale, Alveolar macrophages prevent lethal influenza pneumonia by inhibiting infection of type-1 alveolar epithelial cells. *PLOS Pathog.* **13**, e1006140 (2017).
 41. X.-Z. J. Guo, P. Dash, J. C. Crawford, E. K. Allen, A. E. Zamora, D. F. Boyd, S. Duan, R. Bajracharya, W. A. Awad, N. Apiwatanakul, P. Vogel, T.-D. Kanneganti, P. G. Thomas, Lung $\gamma\delta$ T cells mediate protective responses during neonatal influenza infection that are associated with type 2 immunity. *Immunity* **49**, 531–544.e6 (2018).
 42. G. Li, L. Zhou, C. Zhang, Y. Shi, D. Dong, M. Bai, R. Wang, C. Zhang, Insulin-like growth factor 1 regulates acute inflammatory lung injury mediated by influenza virus infection. *Front. Microbiol.* **10**, 2541 (2019).
 43. C. Schneider, S. P. Nobs, A. K. Heer, M. Kurrer, G. Klinke, N. van Rooijen, J. Vogel, M. Kopf, Alveolar macrophages are essential for protection from respiratory failure and associated morbidity following influenza virus infection. *PLOS Pathog.* **10**, e1004053 (2014).
 44. C. M. Carlson, E. A. Turpin, L. A. Moser, K. B. O'Brien, T. D. Cline, J. C. Jones, T. M. Tumpey, J. M. Katz, L. A. Kelley, J. Gaudie, S. Schultz-Cherry, Transforming growth factor- β : Activation by neuraminidase and role in highly pathogenic H5N1 influenza pathogenesis. *PLOS Pathog.* **6**, e1001136 (2010).
 45. F. Coulombe, J. Jaworska, M. Verway, F. Tzelepis, A. Massoud, J. Gillard, G. Wong, G. Kobinger, Z. Xing, C. Couture, P. Joubert, J. H. Fritz, W. S. Powell, M. Divangahi, Targeted prostaglandin E2 inhibition enhances antiviral immunity through induction of type I interferon and apoptosis in macrophages. *Immunity* **40**, 554–568 (2014).

46. L. A. Monticelli, G. F. Sonnenberg, M. C. Abt, T. Alenghat, C. G. K. Ziegler, T. A. Doering, J. M. Angelosanto, B. J. Laidlaw, C. Y. Yang, T. Sathaliyawala, M. Kubota, D. Turner, J. M. Diamond, A. W. Goldrath, D. L. Farber, R. G. Collman, E. J. Wherry, D. Artis, Innate lymphoid cells promote lung-tissue homeostasis after infection with influenza virus. *Nat. Immunol.* **12**, 1045–1054 (2011).
47. G. Zhao, A. I. Weiner, K. M. Neupauer, M. F. de Mello Costa, G. Palashikar, S. Adams-Tzivelekidis, N. S. Mangalmurti, A. E. Vaughan, Regeneration of the pulmonary vascular endothelium after viral pneumonia requires COUP-TF2. *Sci Adv* **6**, eabc4493 (2020).
48. K. L. Lin, Y. Suzuki, H. Nakano, E. Ramsburg, M. D. Gunn, CCR2⁺ monocyte-derived dendritic cells and exudate macrophages produce influenza-induced pulmonary immune pathology and mortality. *J. Immunol.* **180**, 2562–2572 (2008).
49. D. Moskophidis, D. Kioussis, Contribution of virus-specific CD8⁺ cytotoxic T cells to virus clearance or pathologic manifestations of influenza virus infection in a T cell receptor transgenic mouse model. *J. Exp. Med.* **188**, 223–232 (1998).
50. L. Turianová, V. Lachová, D. Svetlíková, A. Kostrábová, T. Betáková, Comparison of cytokine profiles induced by nonlethal and lethal doses of influenza A virus in mice. *Exp. Ther. Med.* **18**, 4397–4405 (2019).
51. J. A. McCullers, The co-pathogenesis of influenza viruses with bacteria in the lung. *Nat. Rev. Microbiol.* **12**, 252–262 (2014).
52. U. Kulkarni, R. L. Zemans, C. A. Smith, S. C. Wood, J. C. Deng, D. R. Goldstein, Excessive neutrophil levels in the lung underlie the age-associated increase in influenza mortality. *Mucosal Immunol.* **12**, 545–554 (2019).
53. B. Zhu, R. Zhang, C. Li, L. Jiang, M. Xiang, Z. Ye, H. Kita, A. M. Melnick, A. L. Dent, J. Sun, BCL6 modulates tissue neutrophil survival and exacerbates pulmonary inflammation following influenza virus infection. *Proc. Natl. Acad. Sci. U.S.A.* **116**, 11888–11893 (2019).
54. M. D. Tate, L. J. Ioannidis, B. Croker, L. E. Brown, A. G. Brooks, P. C. Reading, The role of neutrophils during mild and severe influenza virus infections of mice. *PLOS ONE* **6**, e17618 (2011).
55. M. H. Askenase, S.-J. Han, A. L. Byrd, D. Moraes da Fonseca, N. Bouladoux, C. Wilhelm, J. E. Konkel, T. W. Hand, N. Lacerda-Queiroz, X. Su, G. Trinchieri, J. R. Grainger, Y. Belkaid, Bone-marrow-resident NK cells prime monocytes for regulatory function during infection. *Immunity* **42**, 1130–1142 (2015).
56. R. Yamamoto, Y. Xu, S. Ikeda, K. Sumida, H. Tanaka, K. Hozumi, A. Takaori-Kondo, N. Minato, Thymic development of a unique bone marrow-resident innate-like T cell subset with a potent innate immune function. *J. Immunol.* **203**, 167–177 (2019).
57. M. Kowanetz, X. Wu, J. Lee, M. Tan, T. Hagenbeek, X. Qu, L. Yu, J. Ross, N. Korsisaari, T. Cao, H. Bou-Reslan, D. Kallop, R. Weimer, M. J. C. Ludlam, J. S. Kaminker, Z. Modrusan, N. van Bruggen, F. V. Peale, R. Carano, Y. G. Meng, N. Ferrara, Granulocyte-colony stimulating factor promotes lung metastasis through mobilization of Ly6G⁺Ly6C⁺ granulocytes. *Proc. Natl. Acad. Sci. U.S.A.* **107**, 21248–21255 (2010).
58. S. B. Coffelt, K. Kersten, C. W. Doornebal, J. Weiden, K. Vrijland, C.-S. Hau, N. J. M. Versteegen, M. Ciampricotti, L. J. A. C. Hawinkels, J. Jonkers, K. E. de Visser, IL-17-producing $\gamma\delta$ T cells and neutrophils conspire to promote breast cancer metastasis. *Nature* **522**, 345–348 (2015).
59. C. Paget, S. Ivanov, J. Fontaine, F. Blanc, M. Pichavant, J. Rensson, E. Bialecki, J. Pothlichet, C. Vendeville, G. Barba-Speath, M.-R. Huerre, C. Faveeuw, M. Si-Tahar, F. Trottein, Potential role of invariant NKT cells in the control of pulmonary inflammation and CD8⁺ T cell response during acute influenza A virus H3N2 pneumonia. *J. Immunol.* **186**, 5590–5602 (2011).
60. M. Hassane, Y. Jouan, F. Creusat, D. Soulard, C. Boisseau, L. Gonzalez, E. C. Patin, N. Heuzé-Vourc'h, J.-C. Sirard, C. Faveeuw, F. Trottein, M. Si-Tahar, T. Baranek, C. Paget, Interleukin-7 protects against bacterial respiratory infection by promoting IL-17A-producing innate T-cell response. *Mucosal Immunol.* **13**, 128–139 (2020).
61. D. Gupta, H. P. Shah, K. Malu, N. Berliner, P. Gaines, Differentiation and characterization of myeloid cells. *Curr Protoc Immunol* **104**, 22F.5.1–22F.5.28 (2014).
62. C. S. McGinnis, L. M. Murrow, Z. J. Gartner, DoubletFinder: Doublet detection in single-cell RNA sequencing data using artificial nearest neighbors. *Cell Syst* **8**, 329–337.e4 (2019).
63. J. Alquicira-Hernandez, J. E. Powell, Nebulosa recovers single-cell gene expression signals by Kernel density estimation. *Bioinformatics* **37**, 2485–2487 (2021).
64. F. A. Wolf, P. Angerer, F. J. Theis, SCANPY: Large-scale single-cell gene expression data analysis. *Genome Biol.* **19**, 15 (2018).

Acknowledgments: We thank the University of Tours (PST-A) and the Institut Pasteur de Lille animal facilities for excellent mouse husbandry. The Cytometry and Single-cell Immunobiology core facility (University of Tours, PST-ASB) is also acknowledged for technical assistance. We are grateful to all health care coworkers involved especially A. Aubrey, D. Chartier, and V. Siméon for excellent management of patient samples and clinical data. S. Ehrmann, P.-F. Dequin, A. Legras, D. Garot, E. Mercier, C. Salmon-Gandonnière, L. Bodet-Contentin, M. Morisseau, S. Mankikian, and W. Darwiche are acknowledged for patient inclusions. We thank all the patients and their families for trust and confidence in our work. **Funding:** This work was supported by the French National Research Agency (ANR) grants: NKTdiff, ANR-19-CE15-0032-01 (C.P.) and ANR-21-CE07-0053 (C.P.); Région Centre Val de Loire grants: Project APR-IA Pirana (C.P.) and Project APR-IR EXASPIR17 (T.B.); Région Centre Val de Loire/European council grant: FEDER EuroFERI (N.W., M.S.-T., and C.P.); Ministère de l'Éducation Nationale de la Recherche et Technique: Doctoral fellowships (F.C. and E.B.); INSERM doctoral fellowships: Poste d'accueil (Y.J. and A.H.); and Fondation du Souffle doctoral fellowship: "Antoine RABBAT" award (Y.J.). **Author contributions:** Conceptualization: Y.J., N.W., F.T., T.M., C.F., T.B., and C.P. Methodology: F.C., Y.J., L.G., A.G., T.M., C.F., T.B., and C.P. Investigation: F.C., Y.J., L.G., E.B., R.L., D.So., A.H., C.B., Q.L., C.d.A.H., V.S., C.F., T.B., and C.P. Validation: F.C., Y.J., L.G., E.B., G.I., R.L., D.So., A.H., M.S.-T., C.F., T.B., and C.P. Formal analysis: F.C., Y.J., L.G., G.I., D.So., A.H., C.d.A.H., C.F., T.B., and C.P. Visualization: Y.J., G.I., and C.P. Project administration: R.L., M.S., T.M., and C.P. Funding acquisition: N.W., M.S., F.T., T.B., and C.P. Supervision: C.P. Software: G.I. Resources: Y.J., E.B., R.L., A.G., Q.L., N.W., D.Si., F.T., B.B., T.M., C.F., and C.P. Writing—original draft: Y.J. and C.P. Writing—review and editing: F.C., Y.J., A.G., C.d.A.H., M.S., B.B., C.F., T.M., and C.P. **Competing interests:** The authors declare that they have no competing interests. **Data and materials availability:** All data needed to evaluate the conclusions in the paper are present in the paper and/or the Supplementary Materials. Single-cell transcriptomic data were available in the Gene Expression Omnibus database under the accession number GSE269075. All R scripts used for single-cell statistical analysis can be accessed on Dryad (doi:10.5061/dryad.280gb5mzw) or GitHub (https://github.com/TEAM-4-CEPR/IFN-g-primes-bone-marrow-neutrophils-for-regulatory-functions-in-severe-viral-pneumonia).

Submitted 4 December 2023
Accepted 11 September 2024
Published 11 October 2024
10.1126/sciadv.adn3257